



1 Modeling canopy-induced turbulence in the Earth system: a unified parameterization of turbulent
2 exchange within plant canopies and the roughness sublayer (CLM-ml v0)

3

4 Gordon B. Bonan¹

5 Edward G. Patton¹

6 Ian N. Harman²

7 Keith W. Oleson¹

8 John J. Finnigan²

9 Yaqiong Lu¹

10 Elizabeth A. Burakowski³

11

12 1 National Center for Atmospheric Research, P. O. Box 3000, Boulder, Colorado, USA 80307

13 2 CSIRO Oceans and Atmosphere, Canberra, Australia

14 3 University of New Hampshire, Durham, New Hampshire, USA

15

16 Corresponding author: G. B. Bonan (bonan@ucar.edu)

17

18

19



20 **Abstract.** Land surface models used in climate models neglect the roughness sublayer and
21 parameterize within-canopy turbulence in an ad hoc manner. We implemented a roughness
22 sublayer turbulence parameterization in a multi-layer canopy model (CLM-ml v0) test if this
23 theory provides a tractable parameterization extending from the ground through the canopy and
24 the roughness sublayer. We compared the canopy model with the Community Land Model
25 (CLM4.5) at 7 forest, 2 grassland, and 3 cropland AmeriFlux sites over a range of canopy height,
26 leaf area index, and climate. The CLM4.5 has pronounced biases during summer months at
27 forest sites in mid-day latent heat flux, sensible heat flux, and gross primary production,
28 nighttime friction velocity, and the radiative temperature diurnal range. The new canopy model
29 reduces these biases by introducing new physics. The signature of the roughness sublayer is most
30 evident in sensible heat flux, friction velocity, and the diurnal cycle of radiative temperature.
31 Within-canopy temperature profiles are markedly different compared with profiles obtained
32 using Monin–Obukhov similarity theory, and the roughness sublayer produces cooler daytime
33 and warmer nighttime temperatures. The herbaceous sites also show model improvements, but
34 the improvements are related less systematically to the roughness sublayer parameterization in
35 these short canopies. The multi-layer canopy with the roughness sublayer turbulence improves
36 simulations compared with the CLM4.5 while also advancing the theoretical basis for surface
37 flux parameterizations.

38

39 **Keywords:** multi-layer canopy, roughness sublayer, Monin–Obukhov similarity theory, wind
40 profile, scalar profile, land surface model

41

42



43

44 **1 Introduction**

45 Distinct parameterizations of land surface processes, separate from the atmospheric physics,
46 were coupled to global climate models in the mid-1980s with the Biosphere–Atmosphere
47 Transfer Scheme (BATS; Dickinson et al., 1986) and the Simple Biosphere Model (SiB; Sellers
48 et al., 1986). While carbon cycle feedbacks have since gained prominence in terms of model
49 development and study of biotic feedbacks with climate change (Friedlingstein et al., 2006,
50 2014), the fundamental coupling between plants and the atmosphere in climate models still
51 occurs with the fluxes of momentum, energy, and mass over the diurnal cycle as mediated by
52 plant physiology, the microclimate of plant canopies, and boundary layer processes. The central
53 paradigm of land surface models, as originally devised by Deardorff (1978) and carried forth
54 with BATS, SiB, and subsequent models, has been to represent plant canopies as a homogeneous
55 “big leaf” without vertical structure, though with separate source fluxes for vegetation and soil.
56 A critical advancement was to analytically integrate leaf physiological processes over profiles of
57 light and nitrogen in the canopy (Sellers et al., 1996) and to extend the canopy to two big leaves
58 to represent sunlit and shaded portions of the canopy (Wang and Leuning, 1998; Dai et al.,
59 2004).

60 In land surface models such as the Community Land Model (CLM4.5; Oleson et al.,
61 2013), for example, fluxes of heat and moisture occur from the leaves to the canopy air, from the
62 ground to the canopy air, and from the canopy air to the atmosphere (Figure 1a). The flux from
63 the canopy to the atmosphere is parameterized using Monin–Obukhov similarity theory (MOST).
64 This theory requires the displacement height (d) and roughness length (z_0). A challenge has
65 been to specify these, which are complex functions of the flow and physical canopy structure



66 (Shaw and Pereira 1982); simple parameterizations calculate them as a fixed fraction of canopy
67 height (as in the CLM4.5) or use relationships with leaf area index (Sellers et al., 1986;
68 Choudhury and Monteith, 1988; Raupach, 1994). An additional challenge, largely ignored in
69 land surface models, is that MOST fails in the roughness sublayer (RSL) extending to twice the
70 canopy height or more (Garratt, 1978; Physick and Garratt, 1995; Harman and Finnigan, 2007,
71 2008). While MOST successfully relates mean gradients and turbulent fluxes in the surface layer
72 above the RSL, within the RSL vertical fluxes are larger than expected from mean gradients
73 obtained using MOST.

74 Dual-source land surface models also require parameterization of turbulent processes
75 within the canopy, where wind speed regulates vegetation fluxes through the leaf boundary layer
76 conductance and where turbulent transport regulates fluxes between the ground and canopy air.
77 Following BATS (Dickinson et al., 1986), the CLM4.5 uses an ad-hoc parameterization without
78 resolving within-canopy profiles of wind speed or turbulence. Wind speed within the canopy is
79 taken as equal to the friction velocity (u_*), and the aerodynamic conductance between the ground
80 and canopy air is proportional to u_* . Zeng et al. (2005) subsequently modified this expression to
81 account for sparse and dense canopies.

82 Harman and Finnigan (2007, 2008) proposed a formulation by which traditional MOST
83 can be modified to account for the RSL. Their theoretical derivations couple the above-canopy
84 turbulent fluxes with equations for the mass and momentum balances within the canopy. Here,
85 we implement and test the theory in a multi-layer canopy model (Bonan et al., 2014). The
86 development of a multi-layer canopy for the ORCHIDEE land surface model has renewed
87 interest in the practical use of this class of canopy models (Ryder et al., 2016; Chen et al., 2016).
88 The earlier multi-layer model development of Bonan et al. (2014) focused on linking stomatal



89 conductance and plant hydraulics and neglected turbulent processes in the canopy. The current
90 work extends the model to include canopy-induced turbulence. The RSL theory avoids a priori
91 specification of z_0 and d by linking these to canopy density and characteristics of the flow;
92 provides consistent forms for various turbulent terms above and within the canopy (friction
93 velocity, wind speed, scalar transfer coefficients); and provides a method for determining the
94 associated profiles of canopy air temperature and water vapor concentration. This study is
95 motivated by the premise that land surface models generally neglect canopy-induced turbulence,
96 that inclusion of this is critical to model simulations, and that the Harman and Finnigan (2007,
97 2008) RSL theory provides a tractable parameterization extending from the ground through the
98 canopy and the RSL.

99

100 **2 Methods**

101 We evaluated the canopy model at 12 AmeriFlux sites comprising 81 site-years of data using the
102 same protocol of the earlier model development (Bonan et al., 2014). We used the 6 forests sites
103 previously described in Bonan et al. (2014) and included additional flux data for 1 forest (US-
104 Dk2), 2 grassland (US-Dk1, US-Var), and 3 cropland sites (US-ARM, US-Bo1, US-Ne3) to test
105 the canopy model over a range of tall and short canopies, dense and sparse leaf area index, and
106 different climates (Table 1). Tower forcing data were from the North American Carbon Program
107 (NACP) site synthesis (Schaefer et al., 2012) as described previously (Bonan et al., 2014), except
108 as noted below for the three Duke tower sites. The model was evaluated using tower
109 observations of net radiation, sensible heat flux, latent heat flux, and friction velocity obtained
110 from the AmeriFlux Level 2 data set (ameriflux.lbl.gov) and with gross primary production from
111 the NACP site synthesis (Schaefer et al., 2012). We limited the simulations to one particular



112 month (with the greatest leaf area) as in Bonan et al. (2014) so as to constrain the model without
113 having to account for seasonal changes in soil water.

114 Ryu et al. (2008) describe the US-Var grassland located in California. The CLM has been
115 previously tested using flux data from the US-Ne3 and US-Bo1 cropland sites (Levis et al.,
116 2012), and we used the same sites here. The US-Ne3 tower site is a rainfed maize (*Zea mays*) –
117 soybean (*Glycine max*) rotation located in Nebraska (Verma et al., 2005). We used flux data for
118 soybean, a C₃ crop (years 2002 and 2004). Kucharik and Twine (2007) give leaf area index, also
119 in the AmeriFlux biological, ancillary, disturbance and metadata. The same ancillary data show a
120 canopy height of 0.9 m during August for soybean. The US-Bo1 site is a maize–soybean rotation
121 located in Illinois (Meyers and Hollinger, 2004; Hollinger et al., 2005). Meyers and Hollinger
122 (2004) give canopy data. We used a leaf area index of 5 m² m⁻² and canopy height of 0.9 m for
123 soybean (1998–2006, even years). Flux data for the US-ARM winter wheat site, used to test the
124 CLM4.5, provides an additional dataset with which to test the model (Lu et al., 2017).

125 Stoy et al. (2006) provide site information for the US-Dk2 deciduous broadleaf forest
126 tower site located in the Duke Forest, North Carolina, which was included here to contrast the
127 adjacent evergreen needleleaf forest and grassland sites. The US-Dk1 tower site in the Duke
128 Forest provides an additional test for grassland (Novick et al., 2004; Stoy et al., 2006). Tower
129 forcing and flux data for 2004–2008 were obtained directly from the tower site investigators
130 (Kim Novick, personal communication).

131

132 **2.1 Model formulation**

133 The canopy model has three main components: leaf gas exchange and plant hydraulics; a
134 numerical solution for scalar profiles within and above the canopy; and inclusion of the RSL



135 parameterization. It builds upon the work of Bonan et al. (2014), which describes leaf gas
136 exchange and plant hydraulics for a multi-layer canopy with sunlit and shaded leaves at each
137 layer in the canopy. Radiative transfer of visible, near-infrared, and longwave radiation is
138 calculated at each level and accounts for forward and backward scattering within the canopy.
139 Bonan et al. (2014) used the radiative transfer model of Norman (1979). We retain that
140 parameterization for longwave radiation, but radiative transfer in the visible and near-infrared
141 wavebands is calculated from the two-stream approximation with the absorbed solar radiation
142 partitioned into direct beam, scattered direct beam, and diffuse radiation for sunlit and shaded
143 leaves in relation to cumulative plant area index as in Dai et al. (2004). This allows better
144 comparison with the CLM4.5, which uses the canopy-integrated two-stream solution for sunlit
145 and shaded leaves. The calculation of leaf temperature and fluxes is solved simultaneously with
146 stomatal conductance, photosynthesis, and leaf water potential in an iterative calculation. This
147 method numerically optimizes water-use efficiency within the constraints imposed by plant
148 water uptake to prevent leaf desiccation using the methodology of Williams et al. (1996). Soil
149 fluxes are calculated using the layer of canopy air immediately above the ground. Bonan et al.
150 (2014) provide further details.

151 Here, we describe the formulation of the scalar profiles and the RSL, which were not
152 included in Bonan et al. (2014). Figure 1 shows the numerical grid. The approach is conceptually
153 similar to the implementation of a multi-layer canopy in ORCHIDEE-CAN and that model's
154 implicit numerical coupling of leaf fluxes and scalar profiles (Ryder et al., 2016; Chen et al.,
155 2016), but modified to include sunlit and shaded leaves at each layer in the canopy and also the
156 RSL (Harman and Finnigan 2007, 2008). The grid spacing (Δz) is 0.5 m for forest and 0.1 m for
157 crop and grassland. We use thin layers to represent the light gradients that drive variation in leaf



158 water potential in the canopy as in Bonan et al. (2014). Indeed, it is this strong variation in leaf
159 water potential from the top of the canopy to the bottom that motivates the need for a multi-layer
160 canopy. Appendix A provides a complete description of the model, and Appendix B lists all
161 model variables.

162

163 **2.1.1 The coupled flux–profile equations**

164 In the volume of air extending from the ground to some reference height above the canopy, the
165 scalar conservation equations for heat and water vapor, the energy balances of the sunlit and
166 shaded canopy, and the ground energy balance provide a system of equations that can be solved
167 for air temperature, water vapor concentration, sunlit and shaded leaf temperatures, and ground
168 temperature. The scalar conservation equation for heat relates the change over some time interval
169 of air temperature (θ , K) at height z (m) to the source fluxes of sensible heat from the sunlit and
170 shaded portions of the canopy ($H_{\ell_{sun}}$ and $H_{\ell_{sha}}$, W m^{-2}) and the vertical flux (H , W m^{-2}). For a
171 vertically-resolved canopy, the one-dimensional conservation equation for temperature is

$$172 \quad \rho_m c_p \frac{\partial \theta(z)}{\partial t} + \frac{\partial H}{\partial z} = [H_{\ell_{sun}}(z) f_{sun}(z) + H_{\ell_{sha}}(z) \{1 - f_{sun}(z)\}] a(z) \quad (1)$$

173 The equivalent equation for water vapor (q , mol mol^{-1}) in relation to the canopy source fluxes
174 ($E_{\ell_{sun}}$ and $E_{\ell_{sha}}$, $\text{mol H}_2\text{O m}^{-2} \text{s}^{-1}$) and vertical flux (E , $\text{mol H}_2\text{O m}^{-2} \text{s}^{-1}$) is

$$175 \quad \rho_m \frac{\partial q(z)}{\partial t} + \frac{\partial E}{\partial z} = [E_{\ell_{sun}}(z) f_{sun}(z) + E_{\ell_{sha}}(z) \{1 - f_{sun}(z)\}] a(z) \quad (2)$$

176 In this notation, ρ_m is molar density (mol m^{-3}) and c_p is the specific heat of air ($\text{J mol}^{-1} \text{K}^{-1}$).

177 $a(z)$ is the plant area density, which is equal to the leaf and stem area increment of a canopy

178 layer divided by the thickness of the layer ($\Delta L(z) / \Delta z$; $\text{m}^2 \text{m}^{-3}$), and f_{sun} is the sunlit fraction of



179 the layer. As in Harman and Finnigan (2007, 2008), the vertical fluxes are parameterized using a
 180 first-order turbulence closure (K-theory) whereby the sensible heat flux is

$$181 \quad H(z) = -\rho_m c_p K_c(z) \frac{\partial \theta}{\partial z} \quad (3)$$

182 and the water vapor flux is

$$183 \quad E(z) = -\rho_m K_c(z) \frac{\partial q}{\partial z} \quad (4)$$

184 with K_c the scalar diffusivity ($\text{m}^2 \text{s}^{-1}$), assumed to be the same for heat and water vapor. These
 185 equations apply above and within the canopy, but with $a(z) = 0$ for layers without vegetation.

186 The source fluxes of sensible heat and water vapor are described by the energy balance
 187 equation and are provided separately for sunlit and shaded fractions of the canopy layer. The
 188 energy balance of sunlit leaves at height z in the canopy is

$$189 \quad c_L(z) \frac{\partial T_{\ell_{sun}}(z)}{\partial t} \Delta L_{sun}(z) = [R_{n\ell_{sun}}(z) - H_{\ell_{sun}}(z) - \lambda E_{\ell_{sun}}(z)] \Delta L_{sun}(z) \quad (5)$$

190 The left-hand side is the storage of heat (W m^{-2}) in a layer of vegetation with heat capacity c_L (J
 191 $\text{m}^{-2} \text{K}^{-1}$), temperature $T_{\ell_{sun}}$ (K), and plant area index $\Delta L_{sun} = f_{sun} \Delta L$ ($\text{m}^2 \text{m}^{-2}$). The right-hand
 192 side is the balance between net radiation ($R_{n\ell_{sun}}$; positive denotes energy gain), sensible heat flux
 193 ($H_{\ell_{sun}}$; positive away from the leaf), and latent heat flux ($\lambda E_{\ell_{sun}}$; positive away from the leaf).

194 The sensible heat flux is

$$195 \quad H_{\ell_{sun}}(z) = 2c_p [T_{\ell_{sun}}(z) - \theta(z)] g_b(z) \quad (6)$$

196 and the evapotranspiration flux is

$$197 \quad E_{\ell_{sun}}(z) = [q_{sat}(T_{\ell_{sun}}) - q(z)] g_{\ell_{sun}}(z) \quad (7)$$



198 For sensible heat, g_b is the leaf boundary layer conductance ($\text{mol m}^{-2} \text{s}^{-1}$), and the factor two
 199 appears because heat transfer occurs from both sides of plant material. The evapotranspiration
 200 flux depends on the saturated water vapor concentration of the leaf, which varies with leaf
 201 temperature and is denoted as $q_{\text{sat}}(T_{\ell_{\text{sun}}})$. It also requires a leaf conductance ($g_{\ell_{\text{sun}}}$, $\text{mol m}^{-2} \text{s}^{-1}$)
 202 that combines evaporation from the wetted fraction of the canopy and transpiration from the dry
 203 fraction. A similar equation applies to shaded leaves. The energy balance given by Eq. (5) does
 204 not account for snow in the canopy, so the simulations are restricted to snow-free periods.

205 These equations are discretized in space and time and are solved in an implicit system of
 206 equations for time $n + 1$. Ryder et al. (2016) and Chen et al. (2016) describe the solution using a
 207 single leaf. Here, the solution is given for separate sunlit and shaded portions of the canopy. In
 208 numerical form and with reference to Figure 1, the scalar conservation equation for temperature
 209 is

$$\begin{aligned}
 210 \quad & \frac{\rho_m \Delta z_i}{\Delta t} c_p (\theta_i^{n+1} - \theta_i^n) - g_{a,i-1} c_p \theta_{i-1}^{n+1} + (g_{a,i-1} + g_{a,i}) c_p \theta_i^{n+1} - g_{a,i} c_p \theta_{i+1}^{n+1} = \\
 & 2g_{b,i} c_p (T_{\ell_{\text{sun},i}}^{n+1} - \theta_i^{n+1}) \Delta L_{\text{sun},i} + 2g_{b,i} c_p (T_{\ell_{\text{sha},i}}^{n+1} - \theta_i^{n+1}) \Delta L_{\text{sha},i}
 \end{aligned} \tag{8}$$

211 and for water vapor is

$$\begin{aligned}
 212 \quad & \frac{\rho_m \Delta z_i}{\Delta t} (q_i^{n+1} - q_i^n) - g_{a,i-1} q_{i-1}^{n+1} + (g_{a,i-1} + g_{a,i}) q_i^{n+1} - g_{a,i} q_{i+1}^{n+1} = \\
 & \left[q_{\text{sat}}(T_{\ell_{\text{sun},i}}^n) + s_i^{\text{sun}} (T_{\ell_{\text{sun},i}}^{n+1} - T_{\ell_{\text{sun},i}}^n) - q_i^{n+1} \right] g_{\ell_{\text{sun},i}} \Delta L_{\text{sun},i} + \\
 & \left[q_{\text{sat}}(T_{\ell_{\text{sha},i}}^n) + s_i^{\text{sha}} (T_{\ell_{\text{sha},i}}^{n+1} - T_{\ell_{\text{sha},i}}^n) - q_i^{n+1} \right] g_{\ell_{\text{sha},i}} \Delta L_{\text{sha},i}
 \end{aligned} \tag{9}$$

213 The first term on the left-hand side of Eq. (8) is the storage of heat (W m^{-2}) over the time interval
 214 Δt (s) in a layer of air with thickness Δz_i (m). The next three terms describe the vertical fluxes
 215 from Eq. (3). These use conductance notation in which g_a is an aerodynamic conductance (mol
 216 $\text{m}^{-2} \text{s}^{-1}$) that is nominally related to $\rho_m K_c / \Delta z$ (Eq. (25) provides the formal relationship). $g_{a,i}$ is



217 the aerodynamic conductance between layer i to $i+1$ above, and $g_{a,i-1}$ is the similar
 218 conductance below between layer i to $i-1$. The two terms on the right-hand side of Eq. (8) are
 219 the vegetation source fluxes of sensible heat for the sunlit and shaded portions of the canopy
 220 layer. Eq. (9) uses comparable terms for water vapor, with $q_{sat}(T_{\ell sun})$ and $q_{sat}(T_{\ell sha})$ linearized as
 221 explained below.

222 The sunlit and shaded temperatures required for Eqs. (8) and (9) are obtained from the
 223 energy balance at canopy layer i . For the sunlit portion of the canopy

$$224 \quad \frac{c_{L,i}}{\Delta t} (T_{\ell sun,i}^{n+1} - T_{\ell sun,i}^n) = R_{n\ell sun,i} - 2g_{b,i}c_p (T_{\ell sun,i}^{n+1} - \theta_i^{n+1}) \quad (10)$$

$$- \lambda \left[q_{sat}(T_{\ell sun,i}^n) + s_i^{sun} (T_{\ell sun,i}^{n+1} - T_{\ell sun,i}^n) - q_i^{n+1} \right] g_{\ell sun,i}$$

225 Latent heat flux uses the linear approximation

$$226 \quad q_{sat}(T_{\ell sun,i}^{n+1}) = q_{sat}(T_{\ell sun,i}^n) + s_i^{sun} (T_{\ell sun,i}^{n+1} - T_{\ell sun,i}^n) \quad (11)$$

227 with $s_i^{sun} = dq_{sat} / dT$ evaluated at $T_{\ell sun,i}^n$. The leaf boundary layer conductance ($g_{b,i}$) depends on
 228 wind speed (u_i , m s⁻¹) as described by Bonan et al. (2014). The conductance for transpiration is
 229 equal to the leaf boundary layer and stomatal conductances acting in series, i.e., $(g_{b,i}^{-1} + g_{sum,i}^{-1})^{-1}$.

230 Here, it is assumed that $g_{b,i}$ is the same for heat and water vapor (as in the CLM4.5). Stomatal

231 conductance ($g_{sum,i}$) is calculated based on water-use efficiency optimization and plant

232 hydraulics (Bonan et al., 2014). The total conductance ($g_{\ell sun,i}$) combines evaporation from the

233 wetted fraction of the plant material ($f_{wet,i}$) and transpiration from the dry fraction ($f_{dry,i}$),

234 similar to that in the CLM4.5 in which

$$235 \quad g_{\ell sun,i} = \left(\frac{g_{sum,i} g_{b,i}}{g_{sum,i} + g_{b,i}} \right) f_{dry,i} + g_{b,i} f_{wet,i} \quad (12)$$



236 with $f_{dry,i} = f_{green,i}(1 - f_{wet,i})$ so that interception occurs from stems and leaves, but transpiration
 237 occurs only from green leaves (denoted by the green leaf fraction $f_{green,i}$). The comparable
 238 equation for shaded leaves is

$$239 \quad \frac{c_{L,i}}{\Delta t} (T_{\ell sha,i}^{n+1} - T_{\ell sha,i}^n) = R_{n\ell sha,i} - 2c_p (T_{\ell sha,i}^{n+1} - \theta_i^{n+1}) g_{b,i} \quad (13)$$

$$- \lambda \left[q_{sat} (T_{\ell sha,i}^n) + s_i^{sha} (T_{\ell sha,i}^{n+1} - T_{\ell sha,i}^n) - q_i^{n+1} \right] g_{\ell sha,i}$$

240 We use post-CLM4.5 changes in intercepted water (W , kg m^{-2}) and the wet and dry fractions of
 241 the canopy (f_{wet} , f_{dry}) that are included in the next version of the model (CLM5).

242 At the lowest layer above the ground ($i = 1$), the ground fluxes H_0 and E_0 are additional
 243 source fluxes, and the ground surface energy balance must be solved to provide the ground
 244 temperature (T_0^{n+1} , K). This energy balance is

$$245 \quad R_{n0} = c_p (T_0^{n+1} - \theta_1^{n+1}) g_{a,0} + \lambda \left\{ h_{s0} \left[q_{sat} (T_0^n) + s_0 (T_0^{n+1} - T_0^n) \right] - q_1^{n+1} \right\} g_{s0}$$

$$+ \frac{\kappa_{soil}}{\Delta z_{soil}} (T_0^{n+1} - T_{soil}^n) \quad (14)$$

246 The first term on the right-hand side is the sensible heat flux between the ground with
 247 temperature T_0 and the air in the canopy layer immediately above the ground with temperature
 248 θ_1 ; $g_{a,0}$ is the corresponding aerodynamic conductance. The second term is the latent heat flux,
 249 with q_1 the water vapor concentration of the canopy air. In calculating soil evaporation, the
 250 surface water vapor concentration is

$$251 \quad q_0^{n+1} = h_{s0} q_{sat} (T_0^{n+1}) = h_{s0} \left[q_{sat} (T_0^n) + s_0 (T_0^{n+1} - T_0^n) \right] \quad (15)$$

252 with $s_0 = dq_{sat} / dT$ evaluated at T_0^n . Evaporation depends on the fractional humidity of the first
 253 soil layer (h_{s0} ; CLM5). The soil evaporative conductance (g_{s0}) is the total conductance and



254 consists of the aerodynamic conductance ($g_{a,0}$) and a soil surface conductance to evaporation
 255 (g_{soil} ; CLM5) acting in series. The last term in Eq. (14) is the heat flux to the soil, which
 256 depends on the thermal conductivity (κ_{soil}), thickness (Δz_{soil}), and temperature (T_{soil}) of the
 257 first soil layer. Eq. (14) does not account for snow on the ground, and the simulations are
 258 restricted to snow-free periods.

259 The numerical solution involves rewriting Eqs. (10) and (13) to obtain expressions for
 260 $T_{sun,i}^{n+1}$ and $T_{sha,i}^{n+1}$ and substituting these in Eqs. (8) and (9). Eqs. (14) and (15) provide the
 261 necessary expressions for T_0^{n+1} and q_0^{n+1} at $i=1$. This gives a tridiagonal system of implicit
 262 equations with the form

$$263 \quad a_{1,i}\theta_{i-1}^{n+1} + b_{11,i}\theta_i^{n+1} + b_{12,i}q_i^{n+1} + c_{1,i}\theta_{i+1}^{n+1} = d_{1,i} \quad (16)$$

$$264 \quad a_{2,i}q_{i-1}^{n+1} + b_{21,i}\theta_i^{n+1} + b_{22,i}q_i^{n+1} + c_{2,i}q_{i+1}^{n+1} = d_{2,i} \quad (17)$$

265 in which $a_{1,i}$, $a_{2,i}$, $b_{11,i}$, $b_{21,i}$, $b_{12,i}$, $b_{22,i}$, $c_{1,i}$, $c_{2,i}$, $d_{1,i}$, and $d_{2,i}$ are algebraic coefficients
 266 (Appendix A1). The system of equations is solved using the method of Richtmyer and Morton
 267 (1967, pp. 275–278), as described in Sect. S1 of the Supplement. θ_i^{n+1} and q_i^{n+1} are obtained for
 268 each level with the boundary conditions θ_{ref}^{n+1} and q_{ref}^{n+1} the temperature and water vapor
 269 concentration at some reference height above the canopy. Then, the leaf temperatures and fluxes
 270 and ground temperature and fluxes are evaluated. Ryder et al. (2016) used a different, but
 271 algebraically equivalent, solution in their model.

272 The equation set has several dependencies that preclude a fully implicit solution for θ_i^{n+1} ,
 273 q_i^{n+1} , $T_{sun,i}^{n+1}$, $T_{sha,i}^{n+1}$, and T_0^{n+1} . Net radiation depends on leaf and ground temperatures. Ryder et al.
 274 (2016) avoided this by specifying longwave emission as an implicit term in the source energy



275 balance equation, but there are other complicating factors. Boundary layer conductance is
276 calculated from wind speed, but also air and leaf temperatures (to account for free convection
277 using the Grashof number). The wet and dry fractions of the canopy vary with evaporative flux.
278 Wind speed and aerodynamic conductances depend on the surface layer stability as quantified by
279 the Obukhov length, yet this length scale depends on the surface fluxes. Stomatal conductance
280 requires leaf temperature, air temperature, and water vapor concentration. Further complexity to
281 the canopy flux calculations arises because stomatal conductance is calculated from principles of
282 water transport along the soil–plant–atmosphere continuum such that leaf water potential cannot
283 drop below some threshold (Williams et al., 1996; Bonan et al., 2014). This requires the leaf
284 transpiration flux, which itself depends on stomatal conductance. The CLM4.5 has similar
285 dependences in its surface flux calculation and solves the fluxes in a numerical procedure with
286 up to 40 iterations for a single model timestep. Instead, we solve the equations using a 5-minute
287 sub-timestep to evaluate fluxes over a full model timestep (30 minutes when coupled to an
288 atmospheric model). In the sub-timestep looping, the current values of wind speed, temperature,
289 water vapor concentration, and canopy water are used to calculate the leaf and aerodynamic
290 conductances needed to update the flux–profiles.

291

292 **2.1.2 Plant canopy and roughness sublayer**

293 The solution to the scalar fluxes and profiles described in the preceding section requires the
294 aerodynamic conductance (g_a), and also wind speed (u) to calculate leaf boundary layer
295 conductance (g_b). These are provided by the RSL parameterization. We follow the theory of
296 Harman and Finnigan (2007, 2008). In their notation, the coordinate system is defined such that
297 the vertical origin is the top of the canopy and z is the deviation from the canopy top. Here, we



298 retain z as the physical height above the ground, whereby $z - h$ is the deviation from the
 299 canopy top. The Harman and Finnigan (2007, 2008) parameterization modifies the MOST
 300 profiles of u , θ , and q above plant canopies for the RSL and does not require a multi-layer
 301 canopy (e.g., Harman, 2012), but was derived by coupling the above-canopy momentum and
 302 scalar fluxes with equations for the momentum and scalar balances within a dense, horizontally
 303 homogenous canopy. Here, we additionally utilize the within-canopy equations.

304 Neglecting the RSL, the wind speed profile is described by MOST as

$$305 \quad u(z) = \frac{u_*}{k} \left[\ln \left(\frac{z-d}{z_0} \right) - \psi_m \left(\frac{z-d}{L_{MO}} \right) + \psi_m \left(\frac{z_0}{L_{MO}} \right) \right] \quad (18)$$

306 where u_* is friction velocity (m s^{-1}), z is height above the ground (m), d is displacement height
 307 (m), z_0 is roughness length (m), and the similarity function ψ_m adjusts the log profile in relation
 308 to the Obukhov length (L_{MO} , m). The Harman and Finnigan (2007, 2008) RSL parameterization
 309 reformulates this as

$$310 \quad u(z) = \frac{u_*}{k} \left[\ln \left(\frac{z-d}{h-d} \right) - \psi_m \left(\frac{z-d}{L_{MO}} \right) + \psi_m \left(\frac{h-d}{L_{MO}} \right) + \hat{\psi}_m \left(\frac{z-d}{L_{MO}}, \frac{z-d}{l_m/\beta} \right) - \hat{\psi}_m \left(\frac{h-d}{L_{MO}}, \frac{h-d}{l_m/\beta} \right) + \frac{k}{\beta} \right] \quad (19)$$

311 This equation is analogous to the previous equation, but is valid only for wind speed above the
 312 canopy at heights $z \geq h$. It rewrites Eq. (18) so that the lower surface is the canopy height (h ,
 313 m) rather than the apparent sink for momentum ($d + z_0$). This eliminates z_0 , but introduces $u(h)$
 314 (the wind speed at the top of the canopy) as a new term, which is specified by $\beta = u_* / u(h)$. Eq.
 315 (19) also introduces $\hat{\psi}_m$, which adjusts the profile to account for canopy-induced physics in the
 316 RSL. Whereas ψ_m uses the length scale L_{MO} , $\hat{\psi}_m$ introduces a second length scale l_m / β . This
 317 length scale is the dominant scale of the shear-driven turbulence generated at or near the canopy



318 top, is equal to $u / (\partial u / \partial z)$ at the top of the canopy, and relates to canopy density. The

319 corresponding equation for temperature above the canopy is

$$320 \quad \theta(z) - \theta(h) = \frac{\theta_*}{k} \left[\ln \left(\frac{z-d}{h-d} \right) - \psi_c \left(\frac{z-d}{L_{MO}} \right) + \psi_c \left(\frac{h-d}{L_{MO}} \right) + \hat{\psi}_c \left(\frac{z-d}{L_{MO}}, \frac{z-d}{l_m / \beta} \right) - \hat{\psi}_c \left(\frac{h-d}{L_{MO}}, \frac{h-d}{l_m / \beta} \right) \right] \quad (20)$$

321 with θ_* a temperature scale (K) and ψ_c and $\hat{\psi}_c$ corresponding functions for scalars. The same

322 equation applies to water vapor, but substituting q and q_* . The new terms in the profile

323 equations introduced by the RSL theory are: β , the ratio of friction velocity to wind speed at the

324 canopy height; l_m , the mixing length (m) in the canopy; and the modified similarity functions

325 $\hat{\psi}_m$ and $\hat{\psi}_c$. Expressions for these are obtained by considering the momentum and scalar

326 balances within a dense, horizontally homogenous canopy and by matching the above- and

327 within-canopy profile equations at the canopy height h (Appendix A2). In addition, the RSL

328 theory provides an equation for d , rather than specifying this as an input parameter. Eq. (20)

329 also requires $\theta(h)$, the air temperature (K) at the canopy height. Harman and Finnigan (2008)

330 provide an equation that relates this to the bulk surface temperature (θ_s) for use with a bulk

331 surface parameterization. Here, we treat $\theta(h)$ as a prognostic variable obtained for the top

332 canopy layer as described in the previous section.

333 With the assumption of a constant mixing length (l_m) in the canopy, wind speed within

334 the canopy at heights $z \leq h$ follows an exponential decline with greater depth in the canopy in

335 relation to the height $z-h$ normalized by the length scale l_m / β , with

$$336 \quad u(z) = u(h) \exp \left[\frac{z-h}{l_m / \beta} \right] \quad (21)$$



337 This is the same equation derived by Inoue (1963) and Cionco (1965), but they express the
 338 exponential term as $-\eta(1-z/h)$, where η is an empirical parameter. Harman and Finnigan
 339 (2007, 2008) introduced the notation l_m/β , whereby $\eta/h = \beta/l_m$, so that the exponential decay
 340 of wind speed in the canopy relates to the RSL. The wind speed profile matches Eq. (19) at the
 341 top of the canopy through $u(h)$. We restrict $u \geq 0.1 \text{ m s}^{-1}$ (see Discussion for further details).
 342 The corresponding profile for the scalar diffusivity within the canopy is similar to that for wind
 343 with

$$344 \quad K_c(z) = K_c(h) \exp\left[\frac{z-h}{l_m/\beta}\right] \quad (22)$$

345 In the RSL theory of Harman and Finnigan (2008),

$$346 \quad K_c(h) = l_m u_* / S_c \quad (23)$$

347 where the Schmidt number (S_c) is defined as the ratio of the diffusivities for momentum and
 348 scalars at the top of the canopy (Appendix A2). The diffusivity of water vapor is assumed to
 349 equal that for heat as in Harman and Finnigan (2008). Eq. (21) for u and Eq. (22) for K_c are
 350 derived from first-order turbulence closure with constant mixing length in the canopy. They have
 351 been used previously to parameterize within-canopy wind and scalar diffusivity in plant canopy
 352 models (Shuttleworth and Wallace, 1985; Choudhury and Monteith, 1988), land surface models
 353 (Dolman, 1993; Bonan, 1996; Niu and Yang, 2004), and hydrologic models (Mahat et al., 2013;
 354 Clark et al., 2015), but without the RSL and with η specified as a model parameter.

355 The aerodynamic conductance for scalars at level i above the canopy ($z > h$) between
 356 heights z_i and z_{i+1} is

$$357 \quad g_{a,i} = \rho_m k u_* \left[\ln\left(\frac{z_{i+1}-d}{z_i-d}\right) - \psi_c\left(\frac{z_{i+1}-d}{L_{MO}}\right) + \psi_c\left(\frac{z_i-d}{L_{MO}}\right) + \hat{\psi}_c(z_{i+1}) - \hat{\psi}_c(z_i) \right]^{-1} \quad (24)$$



358 where $\hat{\psi}_c$ is evaluated at z_i and z_{i+1} . The conductance within the canopy ($z < h$) consistent with
 359 the RSL theory is obtained from Eq. (22) as

$$360 \quad \frac{1}{g_{a,i}} = \frac{1}{\rho_m} \int_{z_i}^{z_{i+1}} \frac{dz}{K_c(z)} \quad (25)$$

361 so that

$$362 \quad \frac{1}{g_{a,i}} = \frac{1}{\rho_m} \frac{S_c}{\beta u_*} \left\{ \exp\left[-\frac{(z_i - h)}{l_m / \beta}\right] - \exp\left[-\frac{(z_{i+1} - h)}{l_m / \beta}\right] \right\} \quad (26)$$

363 For the top canopy layer, the conductance is integrated between the heights z_i and h , and the
 364 above-canopy conductance from h to z_{i+1} is additionally included. The conductance
 365 immediately above the ground is

$$366 \quad g_{a,0} = \rho_m k^2 u_1 \left[\ln\left(\frac{z_1}{z_{0m}}\right) \ln\left(\frac{z_1}{z_{0c}}\right) \right]^{-1} \quad (27)$$

367 with $z_{0m} = 0.01$ m and $z_{0c} = 0.1z_{0m}$ the roughness lengths of the ground for momentum and
 368 scalars, respectively, and assuming neutral stability in this layer. In calculating the conductances,
 369 we use the constraint $\rho_m / g_{a,i} \leq 500$ s m⁻¹ (see Discussion for further details).

370 Harman and Finnigan (2007, 2008) provide a complete description of the RSL equations
 371 and their derivation. Appendix A2 gives the necessary equations as implemented herein. Use of
 372 the RSL parameterization requires specification of the Monin–Obukhov functions ψ_m and ψ_c ,
 373 the RSL functions $\hat{\psi}_m$ and $\hat{\psi}_c$, and equations for β and S_c . Expressions for l_m and d are
 374 obtained from β . Solution to the RSL parameterization requires an iterative calculation for the
 375 Obukhov length (L_{MO}) as shown in Figure 2 and explained further in Appendix A3. The



376 equations as described above apply to dense canopies. Appendix A4 gives a modification for
377 sparse canopies.

378

379 **2.1.3 Plant area density**

380 Land surface models commonly combine leaf and stem area into a single plant area index to
381 calculate radiative transfer, and the CLM4.5 does the same. By using plant area index, big-leaf
382 canopy models assume that woody phytoelements (branches, stems) are randomly interspersed
383 among leaves. Some studies of forest canopies suggest that branches and stems are shaded by
384 foliage and therefore contribute much less to obscuring the sky than if they were randomly
385 dispersed among foliage (Norman and Jarvis, 1974; Kucharik et al., 1998). To allow for shading,
386 we represent plant area density as separate profiles of leaf and stem area. The beta distribution
387 probability density function provides a continuous profile of leaf area density for use with multi-
388 layer canopy models, and we use a uniform profile for stem area, whereby

$$389 \quad a(z) = \frac{L_T}{h} \frac{(z/h)^{p-1} (1-z/h)^{q-1}}{B(p, q)} + \frac{S_T}{h} \quad (28)$$

390 The first term on the right-hand side is the leaf area density with z/h the relative height in the
391 canopy and L_T leaf area index ($\text{m}^2 \text{m}^{-2}$). The beta function (B) is a normalization constant. The
392 parameters p and q determine the shape of the profile (Figure 3). Representative values are
393 $p = q = 2.5$ for grassland and cropland, $p = 3.5$ and $q = 2.0$ for deciduous trees and spruce
394 trees, and $p = 11.5$ and $q = 3.5$ for pine trees (Meyers et al., 1998; Wu et al., 2003). The second
395 term on the right-hand side is the stem area density calculated from the stem area index of the
396 canopy (S_T). For these simulations, L_T comes from tower data (Table 1), and S_T is estimated
397 from L_T as in the CLM4.5.



398

399 **2.1.4 Leaf heat capacity**

400 The CLM4.5 requires specific leaf area as an input parameter, and we use this to calculate leaf
 401 heat capacity (per unit leaf area). Specific leaf area, as used in the CLM4.5, is the area of a leaf
 402 per unit mass of carbon ($\text{m}^2 \text{g}^{-1} \text{C}$) and is the inverse of leaf carbon mass per unit area (M_a , g C
 403 m^{-2}). This latter parameter is converted to dry mass assuming the carbon content of dry biomass
 404 is 50% so that the leaf dry mass per unit area is M_a / f_c with $f_c = 0.5 \text{ g C g}^{-1}$. The leaf heat
 405 capacity (c_L , $\text{J m}^{-2} \text{K}^{-1}$) is calculated from leaf dry mass per unit area after adjusting for the mass
 406 of water, as in Ball et al. (1988) and Blanken et al. (1997). Following Ball et al. (1988), we
 407 assume that the specific heat of dry biomass is one-third that of water ($c_{dry} = 1.396 \text{ J g}^{-1} \text{K}^{-1}$).

408 Then, with f_w the fraction of fresh biomass that is water, the leaf heat capacity is

$$409 \quad c_L = \frac{M_a}{f_c} c_{dry} + \frac{M_a}{f_c} \left(\frac{f_w}{1-f_w} \right) c_{wat} \quad (29)$$

410 The first term on the right-hand side is the mass of dry biomass multiplied by the specific heat of
 411 dry biomass. The second term is the mass of water multiplied by the specific heat of water
 412 ($c_{wat} = 4.188 \text{ J g}^{-1} \text{K}^{-1}$). We assume that 70% of fresh biomass is water ($f_w = 0.7 \text{ g H}_2\text{O g}^{-1}$).
 413 Niinemets (1999) reported a value of $0.66 \text{ g H}_2\text{O g}^{-1}$ in an analysis of leaves from woody plants.
 414 The calculated heat capacity for grasses, crops, and trees is $745\text{--}2792 \text{ J m}^{-2} \text{K}^{-1}$ depending on
 415 specific leaf area (Table 2). For comparison, Blanken et al. (1997) calculated a heat capacity of
 416 $1999 \text{ J m}^{-2} \text{K}^{-1}$ for aspen leaves with a leaf mass per area of 111 g m^{-2} and $f_w = 0.8$. Ball et al.
 417 (1988) reported a range of $1100\text{--}2200 \text{ J m}^{-2} \text{K}^{-1}$ for mangrove leaves spanning a leaf mass per
 418 area of $93\text{--}189 \text{ g m}^{-2}$ with $f_w = 0.71$.



419

420 **2.2 Model simulations**

421 We performed several model simulations to compare the CLM4.5 with the RSL enabled multi-
422 layer canopy and to incrementally evaluate the effect of specific processes on model
423 performance. Table 3 summarizes the major model differences, and Table 4 summarizes the
424 model simulations. The simulations discussed herein are:

- 425 1. CLM4.5 – Simulations with the CLM4.5 using tower meteorology and site data for leaf area
426 index, stem area index, and canopy height.
- 427 2. m0 – This uses the multi-layer canopy, but configured to be similar to the CLM4.5 for leaf
428 biophysics as described in Table 3. Stomatal conductance is calculated as in the CLM4.5.
429 Leaf nitrogen declines exponentially with greater cumulative plant area index from the
430 canopy top with the decay coefficient $K_n = 0.3$ as in the CLM4.5. The nitrogen profile
431 determines the photosynthetic capacity at each layer so that leaves in the upper canopy have
432 greater maximum photosynthetic rates than leaves in the lower canopy. In addition, leaf and
433 stem area are comingled in the CLM4.5, and there is no heat storage in plant biomass. These
434 features are replicated by having a uniform plant area density profile and by setting leaf heat
435 capacity to a small, non-zero number. This simulation excludes a turbulence parameterization
436 so that air temperature, water vapor concentration, and wind speed in the canopy are equal to
437 the reference height forcing. Juang et al. (2008) referred to this as the well-mixed
438 assumption. In this configuration, the fluxes of sensible and latent heat above the canopy are
439 the sum of the source fluxes in the canopy, and friction velocity is not calculated. This is the
440 baseline model configuration.



441 3. m1 – As in m0, but introducing a turbulence closure in the absence of the RSL. Eqs. (16) and
442 (17) are used to calculate θ and q . The CLM4.5 MOST parameterization is used to
443 calculate u and g_a above the canopy. Within the canopy, the mixing length model with
444 exponential profiles for u and g_a as in Eqs. (21) and (26) is used, but with $\eta = 3$, which is a
445 representative value found in many observational studies of wind speed in plant canopies
446 (Thom, 1975; Cionco, 1978; Brutsaert, 1982).

447 The multi-layer canopy model has several changes to leaf biophysics compared with the
448 CLM4.5. These differences are individually examined in the simulations:

449 4. b1 – As in m1, but with stomatal conductance calculated using water-use efficiency and plant
450 hydraulics as in Bonan et al. (2014).

451 5. b2 – As in b1, but with K_n dependent on photosynthetic capacity (V_{cmax}) as in Bonan et al.
452 (2014).

453 6. b3 – As in b2, but with plant area density calculated from Eq. (28).

454 7. b4 – As in b3, but with leaf heat capacity from Eq. (29). This represents the full suite of
455 parameterization changes prior to inclusion of the RSL. We refer to this simulation also as
456 ML-RSL.

457 The final two simulations examine the RSL:

458 8. r1 – As in b4, but with the RSL parameterization used to calculate u and g_a above the
459 canopy using Eqs. (19) and (24). In this configuration, the CLM4.5 MOST parameterization
460 is replaced by the RSL parameterization for above-canopy profiles, but $\eta = 3$ for within
461 canopy profiles.



462 9. r_2 – As in r_1 , but u and g_a in the canopy are calculated from the RSL parameterization
463 using l_m / β rather than $\eta = 3$. This is the full ML+RSL configuration, and comparison with
464 ML-RSL shows the effects of including the RSL parameterization.

465 Simulations were evaluated in terms of net radiation, sensible heat flux, latent heat flux,
466 gross primary production, friction velocity, and radiative temperature. Radiative temperature for
467 both the observations and simulations was evaluated from the upward longwave flux using an
468 emissivity of one. The simulations were assessed in terms of root mean square error (RMSE) for
469 each of the 81 site–years. We additionally assessed model performance using Taylor diagrams
470 and the corresponding skill score (Taylor, 2001) as in Bonan et al. (2014). Taylor diagrams
471 quantify the degree of similarity between the observed and simulated time series of a particular
472 variable in terms of the correlation coefficient (r) and the standard deviation of the model data
473 relative to that of the observations ($\hat{\sigma}$). The Taylor skill score combines these two measures into
474 a single metric of model performance with a value of one when $r = 1$ and $\hat{\sigma} = 1$.

475

476 **3 Results**

477 The ML+RSL simulation has better skill compared with CLM4.5 at most sites and for most
478 variables (Table 5). Of the 7 forest sites, net radiation (R_n) is improved at 5 sites, sensible heat
479 flux (H) at 5 sites, latent heat flux (λE) at 4 sites, friction velocity (u_*) at 6 sites, radiative
480 temperature (T_{rad}) at the 5 sites with data, and gross primary production (GPP) at 3 of the 5 sites
481 with data. H is improved at all 5 herbaceous sites, λE at 3 sites, u_* at 3 sites, T_{rad} at 4 sites,
482 and GPP at the 2 sites with data. R_n generally is unchanged at the herbaceous sites.



483 Simulations for US-UMB illustrate these improvements for the forest sites, where the
484 influence of the RSL is greatest. For July 2006, CLM4.5 overestimates mid-day H and
485 underestimates mid-day GPP (Figure 4). Mid-day latent heat flux is biased low, but within the
486 measurement error. u_* is underestimated at night, and T_{rad} has a larger diurnal range with colder
487 temperatures at night and warmer temperatures during the day compared with the observations.
488 ML+RSL improves the simulation. Mid-day H decreases and GPP increases, nighttime u_*
489 increases, and the diurnal range of T_{rad} decreases. Taylor diagrams for all years (1999–2006;
490 Figure 5) show improved H , λE , and GPP (in terms of the variance of the modeled fluxes
491 relative to the observations), u_* (in terms of correlation with the observations), and T_{rad} (both
492 variance and correlation). Similar improvements are seen at the other forest sites.

493 The observations have a distinct relationship between H and the temperature difference
494 between the surface and reference height ($T_{rad} - T_{ref}$), as shown in Figure 6 for two forest sites
495 (US-UMB and US-Me2) and one crop site (US-ARM) where the root mean square error of the
496 model (ML+RSL) is low for H and T_{rad} . The observations show a positive correlation between
497 $T_{rad} - T_{ref}$ and H beginning at about -2 °C. CLM4.5 and ML+RSL capture this relationship, but
498 the slope at the forest sites is smaller for CLM4.5 than for ML+RSL and the data have more
499 scatter. The observations show a complex relationship between temperature and H for stable
500 conditions ($H < 0$). At the forest sites, CLM4.5 shows a slight linear increase in sensible heat
501 transfer to the surface (US-UMB) or is nearly invariant (US-Me2) as T_{rad} becomes progressively
502 colder than T_{ref} . ML+RSL better captures the observations, particularly the more negative H as
503 $T_{rad} - T_{ref}$ approaches zero. CLM4.5 also has a wider range of temperatures compared with the
504 observations and ML+RSL at the forest sites. Both models perform similarly at US-ARM.



505 Comparisons of ML-RSL and ML+RSL for US-UMB (July 2006) show improvements in
506 the multi-layer canopy even without the RSL parameterization (Figure 4). ML-RSL reduces mid-
507 day H , increases mid-day λE and GPP, and reduces the diurnal range of T_{rad} . The nighttime
508 bias in u_* also decreases. Inclusion of the RSL (ML+RSL) further improves u_* and T_{rad} , but
509 slightly degrades H by increasing the daytime peak.

510 Comparison of the suite of simulations (m0 to r2; Table 4) for forest sites highlights the
511 effect of specific parameterization changes on model performance. The m0 simulation without a
512 turbulence closure has high RMSE compared with CLM4.5 for λE (Figure 7) and H (Figure 8).
513 Inclusion of a turbulence closure (above-canopy, CLM4.5 MOST; within-canopy, mixing length
514 model) in m1 substantially reduces RMSE compared with m0 at all sites. The m1 RMSE for λE
515 is reduced compared with CLM4.5 at 5 of the 7 sites and for H at 4 sites. The leaf biophysical
516 simulations (b1–b4) reduce λE RMSE compared with m1 at 6 sites (US-Ho1 is the exception),
517 and the RMSE also decreases compared with CLM4.5 (Figure 7). Among b1–b4, the biggest
518 effect on λE RMSE occurs from stomatal conductance and nitrogen profiles (b1 and b2). The
519 RSL parameterization (r1 and r2) has relatively little additional effect on RMSE. The leaf
520 biophysical simulations (b1–b4) have a similar effect to reduce RMSE for H compared with
521 m1, and RMSE decreases compared with CLM4.5 (Figure 8). Inclusion of the RSL (r1 and r2)
522 degrades H in terms of RMSE. Whereas the b4 simulation without the RSL parameterization
523 decreases RMSE compared with CLM4.5, this reduction in RMSE is lessened in r1 and r2. The
524 RMSE for u_* in m1 decreases compared with CLM4.5 at all sites (Figure 9). The leaf biophysics
525 simulations have little effect on RMSE, but the RSL simulations (r1 and r2) further reduce
526 RMSE.



527 The m0 simulation without a turbulence closure has substantially lower RMSE for T_{rad}
528 compared with the other simulations (Figure 10). This is seen in an improved simulation of the
529 diurnal temperature range, with warmer nighttime minimum and cooler daytime maximum
530 temperatures compared with the other simulations (not shown). The m1 simulation increases
531 RMSE, but RMSE is still reduced compared with CLM4.5 at the 5 sites with data. The leaf
532 biophysical simulations (b1–b4) have little effect on T_{rad} , but the RSL simulations reduce
533 RMSE, more so for r1 than r2. Leaf temperature profiles are consistent with these results, as
534 shown in Figure 11 for US-UMB. The m0 simulation has the coolest daytime and warmest
535 nighttime leaf temperatures. Inclusion of a turbulence closure (m1) warms daytime temperatures
536 and cools nighttime temperatures. The leaf biophysics (b4) reduces the m1 temperature changes,
537 and the RSL simulations (r1 and r2) further reduce the changes.

538 Wind speed and temperature profiles simulated with the RSL parameterization are
539 noticeably different compared with MOST profiles, as shown in Figure 12 for US-UMB. At mid-
540 day, wind speed in the upper canopy is markedly lower than for MOST, but whereas wind speed
541 goes to zero with MOST, the RSL wind speed remains finite. Mid-day MOST air temperature in
542 the canopy increases monotonically to a maximum of 28.5 °C, but the RSL produces a more
543 complex profile with a temperature maximum of about 26.5 °C in the mid-canopy and lower
544 temperatures near the ground. During the night, the upper canopy cools to a temperature of about
545 15 °C, but temperatures in the lower canopy remain warm. The other forest sites show similar
546 profiles.

547

548 **4 Discussion**



549 The multi-layer canopy with the RSL (ML+RSL) improves the simulation of surface fluxes
550 compared to the CLM4.5 at most forest and herbaceous sites (Table 5). In terms of λE , the
551 turbulence closure using the CLM4.5 MOST above the canopy and a mixing length model in the
552 canopy (with $\eta = 3$) substantially reduces RMSE compared to the well-mixed assumption in
553 which the canopy has the same temperature, water vapor concentration, and wind speed as the
554 reference height (m_0 , m_1 ; Figure 7). A similar result is seen for H (Figure 8). This finding is
555 consistent with Juang et al. (2008), who showed that first-order turbulence closure improves
556 simulations in a multi-layer canopy compared with the well-mixed assumption.

557 Additional improvement in λE comes from the leaf biophysics (particularly stomatal
558 conductance and photosynthetic capacity) (b_1 , b_2 ; Figure 7). This is consistent with Bonan et al.
559 (2014), who previously showed improvements arising from the multi-layer canopy, stomatal
560 conductance, and photosynthetic capacity at the forest sites. Differences between the CLM4.5
561 and ML+RSL stomatal models likely reflects differences in parameters (slope g_1 for CLM4.5;
562 marginal water-use efficiency ι for ML+RSL) rather than model structure (Franks et al., 2017).
563 Further differences arise from the plant hydraulics (Bonan et al., 2014). The RSL has
564 comparatively little effect on λE (r_1 , r_2 ; Figure 7). H is similarly improved by the leaf
565 biophysics, but is degraded by the RSL (Figure 8) because of an increase in the peak mid-day
566 flux. Harman (2012) also found that the RSL has negligible effect on λE because this flux is
567 dominated by stomatal conductance, but increases the peak H .

568 The influence of the RSL is evident in the improved relationship between H and the
569 surface–air temperature difference ($T_{rad} - T_{ref}$) at forest sites (Figure 6). In the CLM4.5, a larger
570 temperature difference is needed to produce the same positive heat flux to the atmosphere
571 compared with the observations. With the RSL, a smaller temperature difference gives the same



572 sensible heat flux, comparable to the observations. This is expected from the RSL theory because
573 of the larger aerodynamic conductance. Similar such improvement is not seen at the crop site
574 (US-ARM) because the measurements were taken above the RSL.

575 The influence of the RSL is also evident in nighttime u_* (Figure 4). Substantial reduction
576 in RMSE is seen in the m1 simulation (Figure 9), which closely mimics the CLM4.5 in terms of
577 leaf biophysics and use of MOST above the canopy. The different numerical methods used
578 between the multi-layer canopy and the CLM4.5 to solve for canopy temperature, surface fluxes,
579 and the Obukhov length may explain the poor CLM4.5 simulations. The RSL parameterization
580 further improves u_* (r1, r2; Figure 9), primarily by increasing u_* at night.

581 Another outcome of the RSL is seen in T_{rad} and leaf temperature. The lowest RMSE
582 occurs with the well-mixed approximation (m0; Figure 10), which also produces the coolest
583 daytime and warmest nighttime leaf temperatures (m0; Figure 11). Adding a turbulence closure
584 (m1) substantially warms daytime leaf temperatures and cools nighttime temperatures, which
585 degrades the T_{rad} RMSE. The RSL (r1, r2) decreases the daytime temperatures and warms the
586 nighttime temperatures, which improve the RMSE. Leaf temperatures are cooler during the day
587 and warmer at night compared with the CLM4.5. Overall, the diurnal temperature range
588 improves in the ML+RSL simulation compared to that from the CLM4.5, seen in both the
589 nighttime minimum and the daytime maximum of T_{rad} (Figure 4). This latter improvement is
590 particularly important given the use of radiometric land surface temperature as an indicator of the
591 climate impacts of land cover change (Alkama and Cescatti, 2016).

592 The simulation of wind and temperature profiles is a key outcome of the multi-layer
593 canopy and RSL. During the day, the CLM4.5 simulates a warmer canopy air space than the
594 ML+RSL simulation (Figure 12). Air temperature obtained from MOST increases monotonically



595 towards the bulk surface, whereas the ML+RSL simulation produces a more complex vertical
596 profile with a maximum located in the upper canopy and cooler temperatures in the lower
597 canopy. Geiger (1927) first described such profiles, seen also in some studies (Jarvis and
598 McNaughton, 1986; Pyles et al., 2000; Staudt et al., 2011). The simulated nighttime temperatures
599 are warmer than the CLM4.5. Temperature profiles have a minimum in the upper canopy, above
600 which temperature increases with height. However, temperatures increase in the lower canopy.
601 Nighttime temperatures in a walnut orchard show a minimum in the upper canopy arising from
602 radiative cooling, but the temperature profile in the lower canopy is more uniform than seen in
603 Figure 12 (Patton et al., 2011). Enhanced diffusivity resulting from convective instability in the
604 canopy makes the temperature profile more uniform in the Patton et al. (2011) observations; this
605 process is lacking in the RSL parameterization. Ryder et al. (2016) and Chen et al. (2016) noted
606 the difficulty in modeling nighttime temperature profiles in forests and introduced in
607 ORCHIDEE-CAN an empirical scaling factor to K_c that varies over the day. The results of the
608 present study, too, suggest that turbulent mixing in conditions where the stratification within and
609 above the canopy differ in sign needs additional consideration. The importance of within-canopy
610 temperature gradients is seen in that the microclimatic influence of dense forest canopies buffers
611 the impact of macroclimatic warming on understory plants (De Frenne et al., 2013) and the
612 vertical climatic gradients in tropical rainforests are steeper than elevation or latitudinal gradients
613 (Scheffers et al., 2013).

614 Various ad hoc changes have been introduced into the next version of the Community
615 Land Model (CLM5) to correct the deficiencies in u_* and T_{rad} . In particular, the Monin–
616 Obukhov stability parameter has been constrained in stable conditions so that $(z-d)/L_{MO} \leq 0.5$.
617 This change increases nighttime u_* , increases sensible heat transfer to the surface at night, and



618 increases nighttime T_{rad} (not shown). In contrast, the ML+RSL simulation reduces these same
619 biases, but resulting from a clear theoretical basis describing canopy-induced physics.

620 The canopy model encapsulates conservation equations for θ and q , the energy balance
621 for the sunlit and shaded canopy, and the ground surface energy balance. The various terms in
622 Eqs. (16) and (17), the governing equations, are easily derived from flux equations and relate to
623 the leaf (g_b , $g_{\ell sun}$, $g_{\ell sha}$) and aerodynamic (g_a) conductances, leaf and canopy air storage terms
624 (c_L , $\rho_m \Delta z / \Delta t$), plant area index and the sunlit fraction (ΔL , f_{sun}), net radiation ($R_{nt sun}$, $R_{nt sha}$),
625 and soil surface (R_{n0} , h_{s0} , g_{s0} , κ_{soil} , T_{soil}). These are all terms that need to be defined in land
626 surface models (except for the storage terms which are commonly neglected), and so the only
627 new term introduced into the flux equations is leaf heat capacity, but that is obtained from the
628 leaf mass per area, which is a required parameter in the CLM4.5.

629 The Harman and Finnigan (2007, 2008) RSL parameterization provides the necessary
630 aerodynamic conductances and wind speed. It produces a comparable representation of surface-
631 atmosphere exchange of heat, water and carbon, including within-canopy exchange, to those
632 based on Lagrangian dynamics (e.g., McNaughton and van den Hurk, 1995) and localized near-
633 field theory (e.g., Raupach, 1989; Raupach et al., 1997; Siqueira et al., 2003; Ryder et al., 2016;
634 Chen et al., 2016). Lagrangian representations have the advantage in that they retain closer
635 fidelity to the underlying dynamics governing exchange. In contrast, however, the RSL
636 formulation provides linked representations for both momentum and (passive) scalar exchange.
637 This coupling, impossible with Lagrangian formulations as there is no locally-conserved
638 equivalent quantity to scalar concentration for momentum, reduces the degrees of freedom
639 involved. The RSL's linked formulation also facilitates the propagation of knowledge about the
640 transport of one quantity onto the transport of all other quantities considered. Unlike Lagrangian



641 formulations, the RSL formulation also naturally asymptotes towards the standard surface layer
642 representations as required, e.g., with increasing height above ground or for short canopies.

643 Furthermore, the components of the RSL formulation are far easier to observe than those
644 in the Lagrangian representations. In particular, the vertical profile of the Lagrangian time scale
645 (T_L), critical to the localized near-field formulation, is extremely difficult to determine from
646 observations or higher-order numerical simulations. Most understanding around T_L is indirect,
647 heuristic, or tied to an inverted model (Massman and Weil, 1999; Haverd et al., 2009). Finally, it
648 is worth noting that the RSL formulation is derived from the scales of the coherent and dominant
649 turbulent structures and directly incorporates canopy architecture (Raupach et al., 1996; Finnigan
650 et al., 2009), thereby permitting future adaptation of the formulation to advances in our
651 understanding of the structure and role of turbulence, e.g. to variation with canopy architecture,
652 landscape heterogeneity, or in low wind conditions. Far greater effort would be required to
653 update the parameterizations of the components in the Lagrangian representations to advances in
654 the understanding of turbulence.

655 The Harman and Finnigan (2007, 2008) RSL parameterization eliminates a priori
656 specification of roughness length and displacement height, but introduces other parameters.
657 Critical parameters are the drag coefficient of canopy elements in each layer ($c_d = 0.25$), the
658 value of $u_* / u(h)$ for neutral conditions ($\beta_N = 0.35$), and the Schmidt number at the canopy top
659 with a nominal value $S_c = 0.5$ as modified for atmospheric stability using Eq. (54). These
660 parameters have physical meaning, are largely observable, have a well-defined range of observed
661 values, and are not unconstrained parameters to fit the model to observations. The expressions
662 for β and S_c given by Eqs. (51) and (54) are observationally-based, but nevertheless are
663 heuristic (Harman and Finnigan, 2007, 2008). The parameter c_2 relates to the depth scale of the



664 RSL and though c_2 can have complex expressions, a simplification is to take $c_2 = 0.5$ (Harman
665 and Finnigan, 2007, 2008; Harman, 2012).

666 The plant canopies simulated in this study are dense canopies in the sense that most of the
667 momentum is absorbed by plant elements. Appendix A4 provides a modification for sparse
668 canopies (e.g., plant area index $< 1 \text{ m}^2 \text{ m}^{-2}$) whereby β decreases, but this extension to sparse
669 canopies is largely untested. Raupach (1994) and Massman (1997) also decrease β with sparse
670 canopies. We note that the same challenge occurs in land surface models such as the CLM4.5,
671 with parameterizations to account for the effects of canopy denseness on within-canopy
672 turbulence (Zeng et al., 2005).

673 The RSL parameterization has limits to its applicability; L_c / L must be greater than some
674 critical value related to β in unstable conditions and less than some critical value in stable
675 conditions (Harman and Finnigan, 2007). We constrained β to a value between 0.5 (unstable)
676 and 0.2 (stable). In practice, this means that $L_c / L \geq -0.79$ (unstable) and $L_c / L \leq 3.75$ (stable),
677 which satisfies the theoretical limits given by Harman and Finnigan (2007). This range of values
678 for β is consistent with observations above forest canopies shown in Harman and Finnigan
679 (2007) and is comparable with other parameterizations. Data presented by Raupach (1994) show
680 a similar range in β for full plant canopies, and his parameterization has a maximum value of
681 0.3. Massman's (1997) parameterization of β has a maximum value of 0.32 for full canopies,
682 but he notes that other studies suggest a range of 0.15–0.25 to 0.40. The Harman and Finnigan
683 (2007) parameterization used here has the advantage of being consistent with current RSL theory
684 (Raupach et al., 1996; Finnigan et al., 2009) and incorporates stability dependence through β , in
685 contrast with Raupach (1994) and Massman (1997). Removing the lower limit $\beta \geq 0.2$ has little



686 effect on the simulations, while the upper limit $\beta \leq 0.5$ acts to suppress daytime u_* at some sites
687 (not shown).

688 l_m / β is a critical length scale in the RSL theory. It modifies flux–profile relationships
689 $(\hat{\phi}_m, \hat{\phi}_c)$ and also the profiles for u and K_c in the canopy given by Eqs. (21) and (22). These
690 latter profiles decline exponentially with greater depth in the canopy in relation to l_m / β , which
691 can be equivalently written as $0.5c_d a / \beta^2$ substituting l_m from Eq. (55) and L_c from Eq. (56).
692 For a particular canopy defined by c_d and $a = (L_r + S_r) / h$, the exponential within-canopy
693 profile is bounded by the limits placed on β . Further insight is gained from an equivalent form
694 of the wind profile equation in which $u(z) = u(h) \exp[-\eta(1 - z/h)]$ with $\eta = h\beta / l_m$. A typical
695 value of η reported in observational studies is 2–4 (Thom, 1975; Cionco, 1978; Brutsaert, 1982).
696 Comparing equations shows that $\eta = 0.5c_d(L_r + S_r) / \beta^2$. The constraint $0.2 \leq \beta \leq 0.5$ places
697 limits to η . The maximum plant area index in our simulations is $7.2 \text{ m}^2 \text{ m}^{-2}$ at US-Dk2. With
698 $c_d = 0.25$, η has values from 3.6 to 22.5. This allows for quite low wind speed and conductance
699 within the canopy. Diabatic stability within the canopy can differ from that above the canopy.
700 This would be reflected in the wind speeds used to calculate the leaf conductances and also the
701 conductance network used to calculate within canopy scalar profiles. For these reasons, we
702 employ minimum values to the within-canopy wind speed and aerodynamic conductances.

703

704 **5 Conclusion**

705 For over 30 years, land surface models have parameterized surface fluxes using a dual-source
706 canopy in which the vegetation is treated as a big-leaf without vertical structure and in which
707 MOST is used to parameterize turbulent fluxes above the canopy. The RSL parameterization of



708 Harman and Finnigan (2007, 2008) provides a means to represent turbulent processes extending
709 from the ground through the canopy and the RSL with sound theoretical underpinnings of
710 canopy-induced turbulence and with few additional parameters. The implementation of the RSL
711 improves model performance in terms of sensible heat flux, friction velocity, and radiative
712 temperature, and additional improvement comes from advances in modeling stomatal
713 conductance and canopy physiology beyond what is in the CLM4.5. Indeed, the modeling of
714 canopy turbulence and canopy physiology are inextricably linked (Finnigan and Raupach 1987),
715 and the 30+ years of land surface models has likely lead to compensating insufficiency in both.

716 Multi-layer canopies are becoming practical for land surface models, seen in the
717 ORCHIDEE-CAN model (Ryder et al., 2016; Chen et al., 2016) and in this study. A multi-layer
718 canopy facilitates the treatment of plant hydraulic control of stomatal conductance (Williams et
719 al., 1996; Bonan et al., 2014), provides new ways to test models directly with leaf-level
720 measurements in the canopy, and is similar to the canopy representations used in canopy-
721 chemistry models (Stroud et al., 2005; Forkel et al., 2006; Wolfe and Thornton, 2011; Ashworth
722 et al., 2015). Here, we provide a tractable means to simulate the necessary profiles of wind
723 speed, temperature, and water vapor. While this is an advancement over the CLM4.5, much work
724 remains to fully develop this class of model. Significant questions remain about how well multi-
725 layer models capture the profiles of air temperature, water vapor, and leaf temperature in the
726 canopy, how important these profiles are for vegetation source fluxes, and how many canopy
727 layers are needed to adequately represent gradients in the canopy. The testing of ORCHIDEE-
728 CAN (Chen et al., 2016) has begun to address these questions, but high quality measurements in
729 canopies are required to better distinguish among turbulence parameterizations (e.g., Patton et
730 al., 2011). Moreover, multi-layer canopies raise a fundamental question about the interface



731 between the atmosphere and land surface. The coupling of the Community Land Model with the
 732 atmosphere depicts the land as a bulk source/sink for heat, moisture, and momentum, and these
 733 fluxes are boundary conditions to the atmosphere model. Multi-layer canopy models simulate a
 734 volume of air extending from some level in the atmosphere to the ground. A critical question that
 735 remains unresolved is where does the parameterization of the atmospheric boundary layer stop
 736 and the land surface model begin.

737

738 **Code availability**

739 The multi-layer canopy runs independent of the CLM4.5, but utilizes common code (e.g., soil
 740 temperature). The canopy flux code is available at https://github.com/gbonan/CLM-ml_v0.

741

742 **Appendix A: Model description**

743 **A1 Derivation of Eqs. (16) and (17)**

744 Eq. (10) for the energy balance of the sunlit portion of layer i can be algebraically rewritten as

$$745 \quad T_{\ell_{sun,i}}^{n+1} = \alpha_i^{sun} \theta_i^{n+1} + \beta_i^{sun} q_i^{n+1} + \delta_i^{sun} \quad (30)$$

746 with

$$747 \quad \alpha_i^{sun} = \frac{2c_p g_{b,i}}{2c_p g_{b,i} + \lambda s_i^{sun} g_{\ell_{sun,i}} + c_{L,i} / \Delta t} \quad (31)$$

$$748 \quad \beta_i^{sun} = \frac{\lambda g_{\ell_{sun,i}}}{2c_p g_{b,i} + \lambda s_i^{sun} g_{\ell_{sun,i}} + c_{L,i} / \Delta t} \quad (32)$$

$$749 \quad \delta_i^{sun} = \frac{R_{n(\ell_{sun,i})} - \lambda \left[q_{sat} \left(T_{\ell_{sun,i}}^n \right) - s_i^{sun} T_{\ell_{sun,i}}^n \right] g_{\ell_{sun,i}} + c_{L,i} T_{\ell_{sun,i}}^n / \Delta t}{2c_p g_{b,i} + \lambda s_i^{sun} g_{\ell_{sun,i}} + c_{L,i} / \Delta t} \quad (33)$$

750 Similar coefficients are found from Eq. (13) for the shaded leaf to give



$$751 \quad T_{\ell_{sha,i}}^{n+1} = \alpha_i^{sha} \theta_i^{n+1} + \beta_i^{sha} q_i^{n+1} + \delta_i^{sha} \quad (34)$$

752 Eq. (14) for the ground surface energy balance is similarly rewritten as

$$753 \quad T_0^{n+1} = \alpha_0 \theta_1^{n+1} + \beta_0 q_1^{n+1} + \delta_0 \quad (35)$$

754 with

$$755 \quad \alpha_0 = \frac{c_p g_{a,0}}{c_p g_{a,0} + \lambda h_{s0} s_0 g_{s0} + \kappa_{soil} / \Delta z_{soil}} \quad (36)$$

$$756 \quad \beta_0 = \frac{\lambda g_{s0}}{c_p g_{a,0} + \lambda h_{s0} s_0 g_{s0} + \kappa_{soil} / \Delta z_{soil}} \quad (37)$$

$$757 \quad \delta_0 = \frac{R_{n0} - \lambda h_{s0} [q_{sat}(T_0^n) - s_0 T_0^n] g_{s0} + T_{soil}^n \kappa_{soil} / \Delta z_{soil}}{c_p g_{a,0} + \lambda h_{s0} s_0 g_{s0} + \kappa_{soil} / \Delta z_{soil}} \quad (38)$$

758 With these substitutions, Eqs. (8) and (9) are rewritten as Eqs. (16) and (17) with the algebraic
 759 coefficients in Sect. S2 of the Supplement.

760

761 **A2 Roughness sublayer parameterization**

762 The flux–gradient relationships used with Monin–Obukhov similarity theory are

$$763 \quad \phi_m(\zeta) = \begin{cases} (1-16\zeta)^{-1/4} & \zeta < 0 \text{ (unstable)} \\ 1+5\zeta & \zeta \geq 0 \text{ (stable)} \end{cases} \quad (39)$$

764 for momentum, and

$$765 \quad \phi_c(\zeta) = \begin{cases} (1-16\zeta)^{-1/2} & \zeta < 0 \text{ (unstable)} \\ 1+5\zeta & \zeta \geq 0 \text{ (stable)} \end{cases} \quad (40)$$

766 for heat and water vapor. These relationships use the dimensionless parameter $\zeta = (z-d) / L_{MO}$.

767 The integrated similarity functions are



$$768 \quad \psi_m(\zeta) = \begin{cases} 2 \ln\left(\frac{1+x}{2}\right) + \ln\left(\frac{1+x^2}{2}\right) - 2 \tan^{-1} x + \frac{\pi}{2} & \zeta < 0 \text{ (unstable)} \\ -5\zeta & \zeta \geq 0 \text{ (stable)} \end{cases} \quad (41)$$

769 with $x = (1 - 16\zeta)^{1/4}$, and

$$770 \quad \psi_c(\zeta) = \begin{cases} 2 \ln\left(\frac{1+x^2}{2}\right) & \zeta < 0 \text{ (unstable)} \\ -5\zeta & \zeta \geq 0 \text{ (stable)} \end{cases} \quad (42)$$

771 These equations are valid for moderate values of ζ from about -2 to 1 (Foken 2006), and we
 772 adopt a similar restriction.

773 The RSL parameterization modifies Monin–Obukhov similarity theory by introducing an
 774 additional dimensionless parameter $\xi = (z - d)\beta / l_m$, which is the height $z - d$ normalized by
 775 the length scale l_m / β . In Harman and Finnigan (2007, 2008), the modified flux–gradient
 776 relationship for momentum is

$$777 \quad \Phi_m(z) = \phi_m\left(\frac{z-d}{L_{MO}}\right) \hat{\phi}_m\left(\frac{z-d}{l_m/\beta}\right) \quad (43)$$

778 with

$$779 \quad \hat{\phi}_m(\xi) = 1 - c_1 \exp(-c_2 \xi) \quad (44)$$

780 and

$$781 \quad c_1 = \left[1 - \frac{k}{2\beta} \phi_m^{-1}\left(\frac{h-d}{L_{MO}}\right) \right] \exp(c_2/2) \quad (45)$$

782 and a simplification is to take $c_2 = 0.5$. The integrated RSL function $\hat{\psi}_m$ is

$$783 \quad \hat{\psi}_m(z) = \int_{z-d}^{\infty} \phi_m\left(\frac{z'}{L_{MO}}\right) \left[1 - \hat{\phi}_m\left(\frac{z'}{l_m/\beta}\right) \right] \frac{dz'}{z'} \quad (46)$$



784 For scalars, the flux–gradient relationship in Harman and Finnigan (2008) is

$$785 \quad \Phi_c(z) = \phi_c \left(\frac{z-d}{L_{MO}} \right) \hat{\phi}_c \left(\frac{z-d}{l_m/\beta} \right) \quad (47)$$

786 The RSL function $\hat{\phi}_c$ is evaluated the same as for $\hat{\phi}_m$ using Eq. (44), but with

$$787 \quad c_1 = \left[1 - \frac{S_c k}{2\beta} \phi_c^{-1} \left(\frac{h-d}{L_{MO}} \right) \right] \exp(c_2/2) \quad (48)$$

788 $\hat{\psi}_c$ is evaluated similar to $\hat{\psi}_m$ using Eq. (46), but with ϕ_c and $\hat{\phi}_c$.

789 The functions $\hat{\psi}_m$ and $\hat{\psi}_c$ must be integrated using numerical methods. In practice,
 790 however, values can be obtained from a look-up table. Eq. (46) can be expanded using Eq. (44)
 791 for $\hat{\phi}_m$ and using $l_m/\beta = 2(h-d)$ from Eq. (57) so that an equivalent equation is

$$792 \quad \hat{\psi}_m(z) = c_1 \int_{z-d}^{\infty} \phi_m \left(\frac{z'}{L_{MO}} \right) \exp \left[-\frac{c_2 z'}{2(h-d)} \right] \frac{dz'}{z'} \quad (49)$$

793 The lower limit of integration in Eq. (49) can be rewritten as $z-d = (z-h) + (h-d)$ and
 794 dividing both sides by $h-d$ gives the expression $(z-h)/(h-d) + 1$. In this notation, Eq. (49)
 795 becomes

$$796 \quad \hat{\psi}_m(z) = c_1 \int_{\frac{z-h}{h-d}+1}^{\infty} \phi_m \left[\frac{(h-d)z'}{L_{MO}} \right] \exp \left(-\frac{c_2 z'}{2} \right) \frac{dz'}{z'} \quad (50)$$

797 In this equation, the integral is specified in a non-dimensional form and depends on two non-
 798 dimensional parameters: $(z-h)/(h-d)$ and $(h-d)/L_{MO}$. The integral is provided in a look-up
 799 table as $A[(z-h)/(h-d), (h-d)/L_{MO}]$. $\hat{\psi}_m$ is then given by $c_1 A$. A similar approach gives $\hat{\psi}_c$.

800 An expression for β is obtained from the relationship



801
$$\beta\phi_m\left(\beta^2L_c/L_{MO}\right)=\beta_N \quad (51)$$

802 with β_N the value of $u_* / u(h)$ for neutral conditions (a representative value is $\beta_N = 0.35$, which

803 is used here). Using Eq. (39) for ϕ_m , the expanded form of Eq. (51) for unstable conditions

804 ($L_{MO} < 0$) is a quadratic equation for β^2 given by

805
$$\left(\beta^2\right)^2+16\frac{L_c}{L_{MO}}\beta_N^4\left(\beta^2\right)-\beta_N^4=0 \quad (52)$$

806 The correct solution is larger of the two roots. For stable conditions ($L_{MO} > 0$), a cubic equation

807 is obtained for β whereby

808
$$5\frac{L_c}{L_{MO}}\beta^3+\beta-\beta_N=0 \quad (53)$$

809 This equation has one real root. We restrict β to be in the range 0.2–0.5 (see Discussion for

810 further details).

811 The Schmidt number (S_c) is parameterized by Harman and Finnigan (2008) as

812
$$S_c=0.5+0.3\tanh\left(2L_c/L_{MO}\right) \quad (54)$$

813 Eq. (21) is derived from the momentum balance equation with a first-order turbulence

814 closure in which the eddy diffusivity is specified in relation to a mixing length (l_m) that is

815 constant with height. From this, Harman and Finnigan (2007) obtained expressions for l_m and d

816 so that

817
$$l_m=2\beta^3L_c \quad (55)$$

818 with

819
$$L_c=\left(c_d a\right)^{-1} \quad (56)$$

820 and



821
$$h - d = \frac{l_m}{2\beta} = \beta^2 L_c \quad (57)$$

822 The term L_c is the canopy length scale (m), specified by the dimensionless leaf aerodynamic
 823 drag coefficient (a common value is $c_d = 0.25$, which is used here) and plant area density (a , m^2
 824 m^{-3}). For Eq. (56), plant area density is estimated as the leaf and stem area index ($L_T + S_T$)
 825 divided by canopy height (h).

826

827 **A3 Obukhov length**

828 The Obukhov length is

829
$$L_{MO} = \frac{u_*^2 \theta_{vref}}{kg \theta_{v*}} \quad (58)$$

830 with θ_{vref} the virtual potential temperature (K) at the reference height, and θ_{v*} the virtual
 831 potential temperature scale (K) given as

832
$$\theta_{v*} = \theta_* + 0.61 \theta_{ref} q_{*,kg} \quad (59)$$

833 The solution to L_{MO} requires an iterative numerical calculation (Figure 2). A value for β is

834 obtained for an initial estimate of L_{MO} using Eq. (51), which gives the displacement height (d)

835 using Eq. (57). The Schmidt number (S_c) is calculated for the current L_{MO} using Eq. (54). The

836 functions ϕ_m and ϕ_c are evaluated using Eqs. (39) and (40) at the canopy height (h) to obtain the

837 parameter c_1 as in Eqs. (45) and (48). The similarity functions ψ_m and ψ_c are evaluated at z

838 and h using Eqs. (41) and (42). The RSL functions $\hat{\psi}_m$ and $\hat{\psi}_c$ are evaluated at z and h from a

839 look-up table. u_* is obtained from Eq. (19) using the wind speed (u_{ref}) at the reference height

840 (z_{ref}). θ_* is calculated from Eq. (20) using θ_{ref} for the current timestep and $\theta(h)$ for the previous



841 sub-timestep, and a comparable equation provides q_* . A new estimate of L_{MO} is obtained, and
842 the iteration is repeated until convergence in L_{MO} is achieved.

843

844 **A4 Sparse canopies**

845 The RSL theory of Harman and Finnigan (2007, 2008) was developed for dense canopies. Sparse
846 canopies can be represented by adjusting β_N , d , and S_c for plant area index ($L_T + S_T$). The
847 neutral value for β is

$$848 \quad \beta_N = [c_\beta + 0.3(L_T + S_T)]^{1/2} \leq \beta_{N\max} \quad (60)$$

849 where

$$850 \quad c_\beta = k^2 \left[\ln \left(\frac{h + z_{0m}}{z_{0m}} \right) \right]^2 \quad (61)$$

851 and $z_{0m} = 0.01$ m is the roughness length for momentum of the underlying ground surface. β_N
852 is constrained to be less than a maximum value for neutral conditions ($\beta_{N\max} = 0.35$). The
853 displacement height is

$$854 \quad h - d = \beta^2 L_c \left\{ 1 - \exp \left[-0.25(L_T + S_T) / \beta^2 \right] \right\} \quad (62)$$

855 The Schmidt number is

$$856 \quad S_c = \left(1 - \frac{\beta_N}{\beta_{N\max}} \right) 1.0 + \frac{\beta_N}{\beta_{N\max}} \left[0.5 + 0.3 \tanh(2L_c / L_{MO}) \right] \quad (63)$$

857 This equation weights the Schmidt number between that for a neutral surface layer (1.0) and the
858 RSL value calculated from Eq. (54).

859

860 **Appendix B: List of symbols, their definition, and units**



Symbol	Description
a_i	Plant area density ($\text{m}^2 \text{m}^{-3}$)
A_n	Leaf net assimilation ($\mu\text{mol CO}_2 \text{m}^{-2} \text{s}^{-1}$)
c_1, c_2	Scaled magnitude (c_1) and height ($c_2 = 0.5$), respectively, for the RSL functions (-)
c_d	Leaf aerodynamic drag coefficient (0.25)
c_{dry}	Specific heat of dry biomass ($1396 \text{ J kg}^{-1} \text{ K}^{-1}$)
$c_{L,i}$	Heat capacity of leaves ($\text{J m}^{-2} \text{ leaf area K}^{-1}$)
c_p	Specific heat of air, $c_{pd}(1 + 0.84q_{ref,kg})M_d$ ($\text{J mol}^{-1} \text{ K}^{-1}$)
c_{pd}	Specific heat of dry air at constant pressure ($1005 \text{ J kg}^{-1} \text{ K}^{-1}$)
c_s	Leaf surface CO_2 concentration ($\mu\text{mol mol}^{-1}$)
c_v	Soil heat capacity ($\text{J m}^{-3} \text{ K}^{-1}$)
c_{wat}	Specific heat of water ($4188 \text{ J kg}^{-1} \text{ K}^{-1}$)
c_β	Parameter for β_N in sparse canopies (-)
d	Displacement height (m)
e_{ref}	Reference height vapor pressure (Pa)
E_i	Water vapor flux ($\text{mol H}_2\text{O m}^{-2} \text{ s}^{-1}$)
E_0	Soil evaporation ($\text{mol H}_2\text{O m}^{-2} \text{ s}^{-1}$)
$E_{c_{sun,i}}, E_{c_{sha,i}}$	Evaporative flux for sunlit or shaded leaves ($\text{mol H}_2\text{O m}^{-2} \text{ plant area s}^{-1}$)
f_c	Carbon content of dry biomass (0.5 g C g^{-1})



$f_{dry,i}$	Dry transpiring fraction of canopy (–)
$f_{green,i}$	Green fraction of canopy (–)
f_i	Leaf nitrogen relative to canopy top (–)
$f_{sun,i}$	Sunlit fraction of canopy (–)
f_w	Water content of fresh biomass ($0.7 \text{ g H}_2\text{O g}^{-1}$)
$f_{wet,i}$	Wet fraction of canopy (–)
g	Gravitational acceleration (9.80665 m s^{-2})
g_0, g_1	Intercept ($\text{mol H}_2\text{O m}^{-2} \text{ s}^{-1}$) and slope (–) for Ball–Berry stomatal conductance
$g_{a,i}$	Aerodynamic conductance ($\text{mol m}^{-2} \text{ s}^{-1}$)
$g_{b,i}$	Leaf boundary layer conductance ($\text{mol m}^{-2} \text{ s}^{-1}$)
$g_{\text{sun},i}, g_{\text{sha},i}$	Leaf conductance for sunlit or shaded leaves ($\text{mol H}_2\text{O m}^{-2} \text{ s}^{-1}$)
g_s	Stomatal conductance ($\text{mol H}_2\text{O m}^{-2} \text{ s}^{-1}$); $g_{\text{sun},i}$, sunlit leaves; $g_{\text{sha},i}$, shaded leaves
g_{s0}	Total surface conductance for water vapor ($\text{mol H}_2\text{O m}^{-2} \text{ s}^{-1}$)
g_{soil}	Soil conductance for water vapor ($\text{mol H}_2\text{O m}^{-2} \text{ s}^{-1}$)
G_0	Soil heat flux (W m^{-2})
h	Canopy height (m)
h_s	Fractional relative humidity at the leaf surface (–)
h_{s0}	Fractional relative humidity at the soil surface (–)
H_i	Sensible heat flux (W m^{-2})



H_0	Soil sensible heat flux (W m^{-2})
$H_{t_{sun,i}}, H_{t_{sha,i}}$	Sensible heat flux for sunlit or shaded leaves (W m^{-2} plant area)
i	Canopy layer index
k	von Karman constant (0.4)
$K_{c,i}$	Scalar diffusivity ($\text{m}^2 \text{s}^{-1}$)
K_n	Canopy nitrogen decay coefficient (–)
l_m	Mixing length for momentum (m)
L_c	Canopy length scale (m)
L_{MO}	Obukhov length (m)
L_r	Canopy leaf area index ($\text{m}^2 \text{m}^{-2}$)
ΔL_i	Canopy layer plant area index ($\text{m}^2 \text{m}^{-2}$)
$\Delta L_{sun,i}, \Delta L_{sha,i}$	Plant area index of sunlit or shaded canopy layer ($\text{m}^2 \text{m}^{-2}$)
\bar{M}	Molecular mass of moist air, ρ / ρ_m (kg mol^{-1})
M_a	Leaf carbon mass per unit area (g C m^{-2} leaf area)
M_d	Molecular mass of dry air ($0.02897 \text{ kg mol}^{-1}$)
M_w	Molecular mass of water ($0.01802 \text{ kg mol}^{-1}$)
n	Time index (–)
P_{ref}	Reference height air pressure (Pa)
q_i	Water vapor concentration (mol mol^{-1})
q_0	Soil surface water vapor concentration (mol mol^{-1})



q_{ref}	Reference height water vapor concentration (mol mol^{-1})
$q_{ref,kg}$	Reference height specific humidity, $0.622e_{ref} / (P_{ref} - 0.378e_{ref})$ (kg kg^{-1})
$q_{sat}(T)$	Saturation water vapor concentration (mol mol^{-1}) at temperature T
q_*	Characteristic water vapor scale (mol mol^{-1})
$q_{*,kg}$	Characteristic water vapor scale, q_*M_w / \bar{M} (kg kg^{-1})
R_{n0}	Soil surface net radiation (W m^{-2})
$R_{n\ell sun,i}$, $R_{n\ell sha,i}$	Net radiation for sunlit or shaded leaves (W m^{-2} plant area)
\mathfrak{R}	Universal gas constant ($8.31446 \text{ J K}^{-1} \text{ mol}^{-1}$)
s_i^{sun} , s_i^{sha}	Temperature derivative of saturation water vapor concentration evaluated at $T_{\ell sun,i}$ and $T_{\ell sha,i}$, dq_{sat} / dT ($\text{mol mol}^{-1} \text{ K}^{-1}$)
s_0	Temperature derivative of saturation water vapor concentration evaluated at the soil surface temperature T_0 , dq_{sat} / dT ($\text{mol mol}^{-1} \text{ K}^{-1}$)
S_c	Schmidt number at the canopy top (–)
S_T	Canopy stem area index ($\text{m}^2 \text{ m}^{-2}$)
t	Time (s)
T_0	Soil surface temperature (K)
$T_{\ell sun,i}$, $T_{\ell sha,i}$	Temperature of sunlit or shaded leaves (K)
T_{ref}	Reference height temperature (K)
T_{soil}	Temperature of first soil layer (K)
u_i	Wind speed (m s^{-1})



u_{ref}	Reference height wind speed (m s^{-1})
u_*	Friction velocity (m s^{-1})
$V_{c\max}$	Maximum carboxylation rate ($\mu\text{mol m}^{-2} \text{s}^{-1}$)
W_i	Intercepted water ($\text{kg H}_2\text{O m}^{-2}$)
z_i	Height (m)
z_{ref}	Reference height (m)
z_{0m}, z_{0c}	Roughness length of ground for momentum (0.01 m) and scalars (0.001 m), respectively
Δz_{soil}	Depth of first soil layer (m)
β	Ratio of friction velocity to wind speed at the canopy height (–)
β_N	Neutral value of β (0.35)
$\beta_{N\max}$	Maximum value of β_N in a sparse canopy (0.35)
ζ	Monin–Obukhov dimensionless parameter (–)
θ_i	Potential temperature (K)
θ_{ref}	Reference height potential temperature (K)
θ_s	Aerodynamic surface temperature (K)
θ_{vref}	Reference height virtual potential temperature (K)
θ_{v*}	Characteristic virtual potential temperature scale (K)
θ_*	Characteristic potential temperature scale (K)
ι	Marginal water-use efficiency parameter ($\mu\text{mol CO}_2 \text{mol}^{-1} \text{H}_2\text{O}$)
κ_{soil}	Thermal conductivity of first soil layer ($\text{W m}^{-1} \text{K}^{-1}$)



ξ	RSL dimensionless parameter (–)
λ	Latent heat of vaporization (45.06802 kJ mol ⁻¹)
ρ	Density of moist air, $\rho_m M_d (1 - 0.378 e_{ref} / P_{ref})$ (mol m ⁻³)
ρ_m	Molar density, $P_{ref} / \mathfrak{R} T_{ref}$ (mol m ⁻³)
ϕ_m, ϕ_c	Monin–Obukhov similarity theory flux–gradient relationships for momentum and scalars (–)
$\hat{\phi}_m, \hat{\phi}_c$	RSL modification of flux–gradient relationships for momentum and scalars (–)
Φ_m, Φ_c	RSL-modified flux–gradient relationships for momentum and scalars (–)
$\psi_\ell, \psi_{\ell\min}$	Leaf water potential and its minimum value (MPa)
ψ_m, ψ_c	Integrated form of Monin–Obukhov stability functions for momentum and scalars (–)
$\hat{\psi}_m, \hat{\psi}_c$	Integrated form of the RSL stability functions for momentum and scalars (–)

861

862 **The Supplement related to this article is available online.**

863

864 *Author contributions.* E. Patton, I. Harman, and J. Finnigan developed the RSL code. G. Bonan

865 developed the numerical solution for scalar profiles in the canopy. G. Bonan and E. Patton

866 implemented the code in the multi-layer canopy. G. Bonan and E. Patton designed the model

867 simulations. K. Oleson performed the CLM4.5 simulations. Y. Lu provided the US-ARM data,

868 and E. Burakowski processed the US-Dk1, US-Dk2, and US-Dk3 data. G. Bonan wrote the

869 manuscript with contributions from all co-authors.

870



871 *Competing interests.* The authors declare that they have no conflict of interest.

872

873 *Acknowledgments.* The National Center for Atmospheric Research is sponsored by the National
874 Science Foundation. This work was supported by the National Science Foundation Science and
875 Technology Center for Multi-Scale Modeling of Atmospheric Processes, managed by Colorado
876 State University under cooperative agreement No. ATM-0425247.

877

878 **References**

879 Alkama, R., and Cescatti, A.: Biophysical climate impacts of recent changes in global forest
880 cover, *Science*, 351, 600–604, 2016.

881 Ashworth, K., Chung, S. H., Griffin, R. J., Chen, J., Forkel, R., Bryan, A. M., and Steiner, A. L.:
882 FORest Canopy Atmosphere Transfer (FORCAST) 1.0: A 1-D model of biosphere–
883 atmosphere chemical exchange, *Geosci. Model Dev.*, 8, 3765–3784, 2015.

884 Ball, M. C., Cowan, I. R., and Farquhar, G. D.: Maintenance of leaf temperature and the
885 optimisation of carbon gain in relation to water loss in a tropical mangrove forest, *Aust. J.*
886 *Plant Physiol.*, 15, 263–276, 1988.

887 Blanken, P. D., Black, T. A., Yang, P. C., Neumann, H. H., Nesic, Z., Staebler, R., den Hartog,
888 G., Novak, M. D., and Lee, X.: Energy balance and canopy conductance of a boreal
889 aspen forest: partitioning overstory and understory components, *J. Geophys. Res.*, 102D,
890 28915–28927, 1997.

891 Bonan, G. B.: A Land Surface Model (LSM Version 1.0) for Ecological, Hydrological, and
892 Atmospheric Studies: Technical Description and User’s Guide, NCAR Tech. Note



- 893 NCAR/TN-417+STR, National Center for Atmospheric Research, Boulder, Colorado,
894 1996.
- 895 Bonan, G. B., Williams, M., Fisher, R. A., and Oleson, K. W.: Modeling stomatal conductance in
896 the earth system: linking leaf water-use efficiency and water transport along the soil–
897 plant–atmosphere continuum, *Geosci. Model Dev.*, 7, 2193–2222, 2014.
- 898 Brutsaert, W.: *Evaporation into the Atmosphere: Theory, History, and Applications*, Kluwer,
899 Dordrecht, 1982.
- 900 Chen, Y., Ryder, J., Bastrikov, V., McGrath, M. J., Naudts, K., Otto, J., Ottlé, C., Peylin, P.,
901 Polcher, J., Valade, A., Black, A., Elbers, J. A., Moors, E., Foken, T., van Gorsel, E.,
902 Haverd, V., Heinesch, B., Tiedemann, F., Knohl, A., Launiainen, S., Loustau, D., Ogée,
903 J., Vesala, T., and Luysaert, S.: Evaluating the performance of land surface model
904 ORCHIDEE-CAN v1.0 on water and energy flux estimation with a single- and multi-
905 layer energy budget scheme, *Geosci. Model Dev.*, 9, 2951–2972, 2016.
- 906 Choudhury, B. J. and Monteith, J. L.: A four-layer model for the heat budget of homogeneous
907 land surfaces, *Q. J. Roy. Meteor. Soc.*, 114, 373–398, 1988.
- 908 Cionco, R. M.: A mathematical model for air flow in a vegetative canopy, *J. Appl. Meteorol.*, 4,
909 517–522, 1965.
- 910 Cionco, R. M.: Analysis of canopy index values for various canopy densities, *Bound.-Lay.*
911 *Meteorol.*, 15, 81–93, 1978.
- 912 Clark, M. P., Nijssen, B., Lundquist, J. D., Kavetski, D., Rupp, D. E., Woods, R. A., Freer, J. E.,
913 Gutmann, E. D., Wood, A. W., Gochis, D. J., Rasmussen, R. M., Tarboton, D. G., Mahat,
914 V., Flerchinger, G. N., and Marks, D. G.: A unified approach for process-based



- 915 hydrologic modeling: 2. Model implementation and case studies, *Water Resour. Res.*, 51,
916 2515–2542, doi:10.1002/2015WR017200, 2015.
- 917 Dai, Y., Dickinson, R. E., and Wang, Y.-P.: A two-big-leaf model for canopy temperature,
918 photosynthesis, and stomatal conductance, *J. Climate*, 17, 2281–2299, 2004.
- 919 Deardorff, J. W.: Efficient prediction of ground surface temperature and moisture, with inclusion
920 of a layer of vegetation, *J. Geophys. Res.*, 83C, 1889–1903, 1978.
- 921 De Frenne, P., Rodríguez-Sánchez, F., Coomes, D. A., Baeten, L., Verstraeten, G., Vellend, M.,
922 Bernhardt-Römermann, M., Brown, C. D., Brunet, J., Cornelis, J., Decocq, G. M.,
923 Dierschke, H., Eriksson, O., Gilliam, F. S., Hédli, R., Heinken, T., Hermy, M., Hommel,
924 P., Jenkins, M. A., Kelly, D. L., Kirby, K. J., Mitchell, F. J. G., Naaf, T., Newman, M.,
925 Peterken, G., Petřík, P., Schultz, J., Sonnier, G., Van Calster, H., Waller, D. M., Walther,
926 G.-R., White, P. S., Woods, K. D., Wulf, M., Graae, B. J., and Verheyen, K.:
927 Microclimate moderates plant responses to macroclimate warming, *Proc. Natl. Acad. Sci.*
928 U.S.A., 110, 18561–18565, 2013.
- 929 Dickinson, R. E., Henderson-Sellers, A., Kennedy, P. J., and Wilson, M. F.: Biosphere–
930 Atmosphere Transfer Scheme (BATS) for the NCAR Community Climate Model, NCAR
931 Tech. Note NCAR/TN-275+STR, National Center for Atmospheric Research, Boulder,
932 Colorado, 1986.
- 933 Dolman, A. J.: A multiple-source land surface energy balance model for use in general
934 circulation models, *Agr. For. Meteorol.*, 65, 21–45, 1993.
- 935 Finnigan J. J. and Raupach M. R.: Transfer processes in plant canopies in relation to stomatal
936 characteristics, in: *Stomatal Function*, edited by: Zeiger, E., Farquhar, G. D., and Cowan,
937 I. R., Stanford University Press, Stanford, Calif., 385–429, 1987.



- 938 Finnigan, J. J., Shaw, R. H., and Patton, E. G.: Turbulence structure above a vegetation canopy,
939 J. Fluid Mech., 637, 387–424, 2009.
- 940 Foken, T.: 50 years of the Monin–Obukhov similarity theory, Bound.-Lay. Meteorol., 119, 431–
941 447, 2006.
- 942 Forkel, R., Klemm, O., Graus, M., Rappenglück, B., Stockwell, W. R., Grabmer, W., Held, A.,
943 Hansel, A., and Steinbrecher, R.: Trace gas exchange and gas phase chemistry in a
944 Norway spruce forest: A study with a coupled 1-dimensional canopy atmospheric
945 chemistry emission model, Atmos. Environ., 40, S28–S42, 2006.
- 946 Franks, P. J., Berry, J. A., Lombardozzi, D. L., and Bonan, G. B.: Stomatal function across
947 temporal and spatial scales: deep-time trends, land-atmosphere coupling and global
948 models, Plant Physiology, 174, 583–602, 2017.
- 949 Friedlingstein, P., Cox, P., Betts, R., Bopp, L., von Bloh, W., Brovkin, V., Cadule, P., Doney, S.,
950 Eby, M., Fung, I., Bala, G., John, J., Jones, C., Joos, F., Kato, T., Kawamiya, M., Knorr,
951 W., Lindsay, K., Matthews, H. D., Raddatz, T., Rayner, P., Reick, C., Roeckner, E.,
952 Schnitzler, K.-G., Schnur, R., Stassmann, K., Weaver, A. J., Yoshikawa, C., and Zeng,
953 N.: Climate–carbon cycle feedback analysis: results from the C⁴MIP model
954 intercomparison, J. Climate, 19, 3337–3353, 2006.
- 955 Friedlingstein, P., Meinshausen, M., Arora, V. K., Jones, C. D., Anav, A., Liddicoat, S. K., and
956 Knutti, R.: Uncertainties in CMIP5 climate projections due to carbon cycle feedbacks, J.
957 Climate, 27, 511–526, 2014.
- 958 Garratt, J. R.: Flux profile relations above tall vegetation, Q. J. Roy. Meteor. Soc., 104, 199–
959 211, 1978.
- 960 Geiger, R.: Das Klima der bodennahen Luftschicht, Friedr. Vieweg & Sohn, Braunschweig,



- 961 Germany, 1927.
- 962 Harman, I. N.: The role of roughness sublayer dynamics within surface exchange schemes,
963 Bound.-Lay. Meteorol., 142, 1–20, 2012.
- 964 Harman, I. N. and Finnigan, J. J.: A simple unified theory for flow in the canopy and roughness
965 sublayer, Bound.-Lay. Meteorol., 123, 339–363, 2007.
- 966 Harman, I. N. and Finnigan, J. J.: Scalar concentration profiles in the canopy and roughness
967 sublayer, Bound.-Lay. Meteorol., 129, 323–351, 2008.
- 968 Haverd, V., Leuning, R., Griffith, D., van Gorsel, E., and Cuntz, M.: The turbulent Lagrangian
969 time scale in forest canopies constrained by fluxes, concentrations and source
970 distributions, Bound.-Lay. Meteorol., 130, 209–228, 2009.
- 971 Hollinger, S. E., Bernacchi, C. J., and Meyers, T. P.: Carbon budget of mature no-till ecosystem
972 in North Central Region of the United States, Agr. For. Meteorol., 130, 59–69, 2005.
- 973 Inoue, E.: On the turbulent structure of airflow within crop canopies, J. Meteorol. Soc. Japan Ser.
974 II, 41, 317–326, 1963.
- 975 Jarvis, P. G. and McNaughton, K. G.: Stomatal control of transpiration: scaling up from leaf to
976 region, Adv. Ecol. Res., 15, 1–49, 1986.
- 977 Juang, J.-Y., Katul, G. G., Siqueira, M. B., Stoy, P. C., and McCarthy, H. R.: Investigating a
978 hierarchy of Eulerian closure models for scalar transfer inside forested canopies, Bound.-
979 Lay. Meteorol, 128, 1–32 (2008).
- 980 Kucharik, C. J. and Twine, T. E.: Residue, respiration, and residuals: evaluation of a dynamic
981 agroecosystem model using eddy flux measurements and biometric data, Agr. For.
982 Meteorol., 146, 134–158, 2007.
- 983 Kucharik, C. J., Norman, J. M., and Gower, S. T.: Measurements of branch area and adjusting



- 984 leaf area index indirect measurements, *Agr. For. Meteorol.*, 91, 69–88, 1998.
- 985 Levis, S., Bonan, G. B., Kluzek, E., Thornton, P. E., Jones, A., Sacks, W. J., and Kucharik, C. J.:
986 Interactive crop management in the Community Earth System Model (CESM1): seasonal
987 influences on land-atmosphere fluxes, *J. Climate*, 25, 4839–4859, 2012.
- 988 Lu, Y., Williams, I. N., Bagley, J. E., Torn, M. S., and Kueppers, L. M.: Representing winter
989 wheat in the Community Land Model (version 4.5), *Geosci. Model Dev.*, 10, 1873–1888,
990 2017.
- 991 Mahat, V., Tarboton, D. G., and Molotch, N. P.: Testing above- and below-canopy
992 representations of turbulent fluxes in an energy balance snowmelt model, *Water Resour.*
993 *Res.*, 49, doi:10.1002/wrcr.20073, 2013.
- 994 Massman, W. J.: An analytical one-dimensional model of momentum transfer by vegetation of
995 arbitrary structure, *Bound.-Lay. Meteorol.*, 83, 407–421, 1997.
- 996 Massman, W. J. and Weil, J. C.: An analytical one-dimensional second-order closure model of
997 turbulence statistics and the Lagrangian time scale within and above plant canopies of
998 arbitrary structure, *Bound.-Lay. Meteorol.*, 91, 81–107, 1999.
- 999 McNaughton, K. G. and van den Hurk, B. J. J. M.: A ‘Lagrangian’ revision of the resistors in the
1000 two-layer model for calculating the energy budget of a plant canopy, *Bound.-Lay.*
1001 *Meteorol.*, 74, 261–288, 1995.
- 1002 Meyers, T. P. and Hollinger, S. E.: An assessment of storage terms in the surface energy balance
1003 of maize and soybean, *Agr. For. Meteorol.*, 125, 105–115, 2004.
- 1004 Meyers, T. P., Finkelstein, P., Clarke, J., Ellestad, T. G., and Sims, P. F.: A multilayer model for
1005 inferring dry deposition using standard meteorological measurements, *J. Geophys. Res.*,
1006 103D, 22645–22661, 1998.



- 1007 Niinemets, Ü.: Components of leaf dry mass per area – thickness and density – alter leaf
1008 photosynthetic capacity in reverse directions in woody plants, *New Phytol.*, 144, 35–47,
1009 1999.
- 1010 Niu, G.-Y. and Yang, Z.-L.: Effects of vegetation canopy processes on snow surface energy and
1011 mass balances, *J. Geophys. Res.*, 109, D23111, doi:10.1029/2004JD004884, 2004.
- 1012 Norman, J. M.: Modeling the complete crop canopy, in: *Modification of the Aerial Environment*
1013 *of Plants*, edited by: Barfield, B. J. and Gerber, J. F., Am. Soc. of Agric. Eng., St. Joseph,
1014 Mich, 249–277, 1979.
- 1015 Norman, J. M. and Jarvis, P. G.: Photosynthesis in Sitka spruce (*Picea sitchensis* (Bong.) Carr.).
1016 III. Measurements of canopy structure and interception of radiation, *J. Appl. Ecol.*, 11,
1017 375–398, 1974.
- 1018 Novick, K. A., Stoy, P. C., Katul, G. G., Ellsworth, D. S., Siqueira, M. B. S., Juang, J., and Oren,
1019 R.: Carbon dioxide and water vapor exchange in a warm temperate grassland, *Oecologia*,
1020 138, 259–274, 2004.
- 1021 Oleson, K. W., Lawrence, D. M., Bonan, G. B., Drewniak, B., Huang, M., Koven, C. D., Levis,
1022 S., Li, F., Riley, W. J., Subin, Z. M., Swenson, S. C., Thornton, P. E., Bozbiyik, A.,
1023 Fisher, R., Heald, C. L., Kluzek, E., Lamarque, J.-F., Lawrence, P. J., Leung, L. R.,
1024 Lipscomb, W., Muszala, S., Ricciuto, D. M., Sacks, W., Sun, Y., Tang, J. and Yang, Z.-
1025 L.: Technical description of version 4.5 of the Community Land Model (CLM), NCAR
1026 Tech. Note NCAR/TN-503+STR, National Center for Atmospheric Research, Boulder,
1027 Colorado, 2013.
- 1028 Patton, E. G., Horst, T. W., Sullivan, P. P., Lenschow, D. H., Oncley, S. P., Brown, W. O.,
1029 Burns, S. P., Guenther, A. B., Held, A., Karl, T., Mayor, S. D., Rizzo, L. V., Spuler, S.



- 1030 M., Sun, J., Turnipseed, A. A., Allwine, E. J., Edburg, S. L., Lamb, B. K., Avissar, R.,
1031 Calhoun, R. J., Kleissl, J., Massman, W. J., Paw U, K. T., and Weil, J. C.: The Canopy
1032 Horizontal Array Turbulence Study. *Bull. Amer. Meteor. Soc.*, 92, 593–611, 2011.
- 1033 Physick, W. L. and Garratt, J. R.: Incorporation of a high-roughness lower boundary into a
1034 mesoscale model for studies of dry deposition over complex terrain, *Bound.-Lay.*
1035 *Meteorol.*, 74, 55–71, 1995.
- 1036 Pyles, R. D., Weare, B. C., and Paw U, K. T.: The UCD Advanced Canopy–Atmosphere–Soil
1037 Algorithm: comparisons with observations from different climate and vegetation regimes,
1038 *Q. J. Roy. Meteor. Soc.*, 126, 2951–2980, 2000.
- 1039 Raupach, M. R.: Simplified expressions for vegetation roughness length and zero-plane
1040 displacement as functions of canopy height and area index, *Bound.-Lay. Meteorol.*, 71,
1041 211–216, 1994.
- 1042 Raupach, M. R.: A practical Lagrangian method for relating scalar concentrations to source
1043 distributions in vegetation canopies, *Q. J. Roy. Meteor. Soc.*, 115, 609–632, 1989.
- 1044 Raupach, M. R., Finnigan, J. J., and Brunet, Y.: Coherent eddies and turbulence in vegetation
1045 canopies: the mixing-length analogy, *Bound.-Lay. Meteorol.*, 78, 351–382, 1996.
- 1046 Raupach, M. R., Finkelde, K., and Zhang, L.: SCAM (Soil-Canopy-Atmosphere Model):
1047 Description and Comparisons with Field Data, Tech. Rep. No. 132, CSIRO Centre for
1048 Environmental Mechanics, Canberra, Australia, 1997.
- 1049 Richardson, A. D., Hollinger, D. Y., Burba, G. G., Davis, K. J., Flanagan, L. B., Katul, G. G.,
1050 Munger, J. W., Ricciuto, D. M., Stoy, P. C., Suyker, A. E., Verma, S. B. and Wofsy, S.
1051 C.: A multi-site analysis of random error in tower-based measurements of carbon and
1052 energy fluxes, *Agric. For. Meteorol.*, 136, 1–18, 2006.



- 1053 Richardson, A. D., Aubinet, M., Barr, A. G., Hollinger, D. Y., Ibrom, A., Lasslop, G., and
1054 Reichstein, M.: Uncertainty quantification, in: Eddy Covariance: A Practical Guide to
1055 Measurement and Data Analysis, edited by: Aubinet, M., Vesala, T. and Papale, D.,
1056 Springer, Dordrecht, 173–209, 2012.
- 1057 Richtmyer, R. D. and Morton, K. W.: Difference Methods for Initial-Value Problems, 2nd ed.,
1058 Wiley, New York, 1967.
- 1059 Ryder, J., Polcher, J., Peylin, P., Ottlé, C., Chen, Y., van Gorsel, E., Haverd, V., McGrath, M. J.,
1060 Naudts, K., Otto, J., Valade, A., and Luysaert, S.: A multi-layer land surface energy
1061 budget model for implicit coupling with global atmospheric simulations, *Geosci. Model*
1062 *Dev.*, 9, 223–245, 2016.
- 1063 Ryu, Y., Baldocchi, D. D., Ma, S., and Hehn, T.: Interannual variability of evapotranspiration
1064 and energy exchange over an annual grassland in California, *J. Geophys. Res.*, 113,
1065 D09104, doi:10.1029/2007JD009263, 2008.
- 1066 Schaefer, K., Schwalm, C. R., Williams, C., Arain, M. A., Barr, A., Chen, J. M., Davis, K. J.,
1067 Dimitrov, D., Hilton, T. W., Hollinger, D. Y., Humphreys, E., Poulter, B., Raczka, B. M.,
1068 Richardson, A. D., Sahoo, A., Thornton, P., Vargas, R., Verbeeck, H., Anderson, R.,
1069 Baker, I., Black, T. A., Bolstad, P., Chen, J., Curtis, P. S., Desai, A. R., Dietze, M.,
1070 Dragoni, D., Gough, C., Grant, R. F., Gu, L., Jain, A., Kucharik, C., Law, B., Liu, S.,
1071 Lokipitiya, E., Margolis, H. A., Matamala, R., McCaughey, J. H., Monson, R., Munger, J.
1072 W., Oechel, W., Peng, C., Price, D. T., Ricciuto, D., Riley, W. J., Roulet, N., Tian, H.,
1073 Tonitto, C., Torn, M., Weng, E., and Zhou, X.: A model–data comparison of gross
1074 primary productivity: results from the North American Carbon Program site synthesis, *J.*
1075 *Geophys. Res.*, 117, G03010, doi:10.1029/2012JG001960, 2012.



- 1076 Scheffers, B. R., Phillips, B. L., Laurance, W. F., Sodhi, N. S., Diesmos, A., and Williams, S. E.:
1077 Increasing arboreality with altitude: a novel biogeographic dimension, *Proc. R. Soc. B*,
1078 280, 20131581, doi:10.1098/rspb.2013.1581, 2013.
- 1079 Sellers, P. J., Mintz, Y., Sud, Y. C., and Dalcher, A.: A simple biosphere model (SiB) for use
1080 within general circulation models, *J. Atmos. Sci.*, 43, 505–531, 1986.
- 1081 Sellers, P. J., Randall, D. A., Collatz, G. J., Berry, J. A., Field, C. B., Dazlich, D. A., Zhang, C.,
1082 Collelo, G. D., and Bounoua, L.: A revised land surface parameterization (SiB2) for
1083 atmospheric GCMs. Part I: Model formulation, *J. Climate*, 9, 676–705, 1996.
- 1084 Shaw, R. H. and Pereira, A. R.: Aerodynamic roughness of a plant canopy: a numerical
1085 experiment, *Agr. Meteorol.*, 26, 51–65, 1982.
- 1086 Shuttleworth, W. J. and Wallace, J. S.: Evaporation from sparse crops – an energy combination
1087 theory, *Q. J. Roy. Meteor. Soc.*, 111, 839–855, 1985.
- 1088 Siqueira, M., Leuning, R., Kolle, O., Kelliher, F. M., and Katul, G. G.: Modelling sources and
1089 sinks of CO₂, H₂O and heat within a Siberian pine forest using three inverse methods, *Q.*
1090 *J. Roy. Meteor. Soc.*, 129, 1373–1393, 2003.
- 1091 Staudt, K., Serafimovich, A., Siebicke, L., Pyles, R. D., and Falge, E.: Vertical structure of
1092 evapotranspiration at a forest site (a case study), *Agr. For. Meteorol.*, 151, 709–729,
1093 2011.
- 1094 Stoy, P. C., Katul, G. G., Siqueira, M. B. S., Juang, J.-Y., Novick, K. A., McCarthy, H. R., Oishi,
1095 A. C., Uebelherr, J. M., Kim, H.-S., and Oren, R.: Separating the effects of climate and
1096 vegetation on evapotranspiration along a successional chronosequence in the southeastern
1097 US, *Global Change Biol.*, 12, 2115–2135, 2006.



- 1098 Stroud, C., Makar, P., Karl, T., Guenther, A., Geron, C., Turnipseed, A., Nemitz, E., Baker, B.,
1099 Potosnak, M., and Fuentes, J. D.: Role of canopy-scale photochemistry in modifying
1100 biogenic-atmosphere exchange of reactive terpene species: Results from the CELTIC
1101 field study, *J. Geophys. Res.*, 110, D17303, doi:10.1029/2005JD005775, 2005.
- 1102 Taylor, K. E.: Summarizing multiple aspects of model performance in a single diagram, *J.*
1103 *Geophys. Res.*, 106D, 7183–7192, 2001.
- 1104 Thom, A. S.: Momentum, mass and heat exchange of plant communities, in: *Vegetation and the*
1105 *Atmosphere: vol. 1. Principles*, edited by: Monteith, J. L., Academic Press, New York,
1106 57–109, 1975.
- 1107 Verma, S. B., Dobermann, A., Cassman, K. G., Walters, D. T., Knops, J. M., Arkebauer, T. J.,
1108 Suyker, A. E., Burba, G. G., Amos, B., Yang, H., Ginting, D., Hubbard, K. G., Gitelson,
1109 A. A., and Walter-Shea, E. A.: Annual carbon dioxide exchange in irrigated and rainfed
1110 maize-based agroecosystems, *Agr. For. Meteorol.*, 131, 77–96, 2005.
- 1111 Wang, Y.-P. and Leuning, R.: A two-leaf model for canopy conductance, photosynthesis and
1112 partitioning of available energy. I: Model description and comparison with a multi-
1113 layered model, *Agr. For. Meteorol.*, 91, 89–111, 1998.
- 1114 Williams, M., Rastetter, E. B., Fernandes, D. N., Goulden, M. L., Wofsy, S. C., Shaver, G. R.,
1115 Melillo, J. M., Munger, J. W., Fan, S.-M., and Nadelhoffer, K. J.: Modelling the soil–
1116 plant–atmosphere continuum in a *Quercus–Acer* stand at Harvard Forest: the regulation
1117 of stomatal conductance by light, nitrogen and soil/plant hydraulic properties, *Plant Cell*
1118 *Environ.*, 19, 911–927, 1996.



- 1119 Wolfe, G. M. and Thornton, J. A.: The Chemistry of Atmosphere–Forest Exchange (CAFE)
1120 model – Part 1: Model description and characterization, *Atmos. Chem. Phys.*, 11, 77–101
1121 (2011).
- 1122 Wu, Y., Brashers, B., Finkelstein, P. L., and Pleim, J. E.: A multilayer biochemical dry
1123 deposition model. 1. Model formulation, *J. Geophys. Res.*, 108D, 4013,
1124 doi:10.1029/2002JD002293, 2003.
- 1125 Zeng, X., Barlage, M., Dickinson, R.E., Dai, Y., Wang, G., and Oleson, K.: Treatment of
1126 undercanopy turbulence in land models, *J. Climate*, 18, 5086–5094, 2005.
- 1127
- 1128
- 1129



1130

1131 Table 1. Site information for the 4 deciduous broadleaf forest (DBF), 3 evergreen needleleaf
1132 forest (ENF), 2 grassland (GRA), and 3 cropland (CRO) flux towers, including mean annual
1133 temperature (MAT) and annual precipitation (Prec).

Site	Veg- etation type	Lat- itude	Long- itude	MAT (°C)	Prec (mm)	Years	Month	Leaf area index ^a	Canopy height (m)
US-Dk2	DBF	35.97	-79.10	14.4	1169	2004– 2008	July	6.2	25
US-Ha1	DBF	42.54	-72.17	6.6	1071	1992– 2006	July	4.9	23
US-MMS	DBF	39.32	-86.41	10.8	1032	1999– 2006	July	4.7	27
US-UMB	DBF	45.56	-84.71	5.8	803	1999– 2006	July	4.2	21
US-Dk3	ENF	35.98	-79.09	14.4	1170	2004– 2008	July	4.7	17
US-Ho1	ENF	45.20	-68.74	5.3	1070	1996– 2004	July	4.6	20
US-Me2	ENF	44.45	-121.56	6.3	523	2002– 2007	July	3.8	14
US-Dk1 ^b	GRA	35.97	-79.09	14.4	1170	2004– 2008	July	1.7	0.5



US-Var	GRA	38.41	-120.95	15.8	559	2001– 2007	March	2.4	0.6
US-ARM	CRO	36.61	-97.49	14.8	843	2003–4, 2006–7, 2009–10	April	2–4	0.5
US-Bo1	CRO	40.01	-88.29	11.0	991	1998– 2006 (even)	August	5.0	0.9
US-Ne3	CRO	41.18	-96.44	10.1	784	2002, 2004	August	3.7	0.9

1134

1135 ^a Shown is the maximum for the month. Maximum leaf area index for US-ARM varied by year,
 1136 and shown is the range in monthly maximum across all years.

1137 ^b H and u_s for 2007 and 2008 are excluded.

1138

1139

1140

1141

1142

1143

1144



1145

1146 Table 2. Leaf heat capacity

Plant functional type	Specific leaf area ($\text{m}^2 \text{g}^{-1} \text{C}$)	Leaf mass per area (g dry mass m^{-2})	Heat capacity ($\text{J m}^{-2} \text{K}^{-1}$)
Grass, crop	0.03	67	745
Deciduous broadleaf tree	0.03	67	745
Evergreen needleleaf tree			
Temperate	0.01	200	2234
Boreal	0.008	250	2792

1147

1148

1149

1150



1151 Table 3. Major differences between the CLM4.5 and ML+RSL

Feature	CLM4.5	ML+RSL
Canopy	Dual source: vegetation (sunlit/shaded big-leaf) and soil	Multilayer; sunlit and shaded leaf fluxes at each level; scalar profiles (u , θ , q) based on conservation equations
Plant area index	Big leaf	Vertical profile uses beta distribution probability density function for leaves and uniform profile for stems
Stomatal conductance	$g_s = g_0 + g_1 h_s A_n / c_s$	$\Delta A_n / \Delta E_\ell = \iota$ with $\psi_\ell > \psi_{\ell \min}$; Bonan et al. (2014)
Relative leaf nitrogen profile $f_i = \exp[-K_n \sum \Delta L_j]$	$K_n = 0.3$	$K_n = \exp(0.00963V_{c \max} - 2.43)$; Bonan et al. (2014)
Storage	–	Plant: $c_L (\Delta T_\ell / \Delta t)$ Air: $\rho_m c_p \Delta z (\Delta \theta / \Delta t)$ Air: $\rho_m \Delta z (\Delta q / \Delta t)$
Above-canopy turbulence	MOST	RSL
Within-canopy turbulence	Understory wind speed equals u_* ; aerodynamic conductance based on u_* and understory Ri.	$u(z) = u(h) \exp[(z-h)\beta/l_m]$ $K_c(z) = K_c(h) \exp[(z-h)\beta/l_m]$



1152 Table 4. Summary of simulation changes to the turbulence parameterization and leaf biophysics

Simulation	Turbulence		Biophysical			
	θ, q	u, g_a	g_s	K_n	Plant area density	c_L
CLM4.5	CLM4.5	CLM4.5	CLM4.5	CLM4.5	$(L_T + S_T) / h$	–
m0	Well-mixed	–	"	"	"	"
m1	Eqs. (16) and (17)	$z > h$: CLM4.5 $z < h$: Eqs. (21) and (26), $\eta = 3$	"	"	"	"
b1	"	"	Bonan et al. (2014)	"	"	"
b2	"	"	"	Bonan et al. (2014)	"	"
b3	"	"	"	"	Eq. (28)	"
b4	"	"	"	"	"	Eq. (29)
r1	"	$z > h$: Eqs. (19) and (24) $z < h$: Eqs. (21) and (26), $\eta = 3$	"	"	"	"
r2	"	"	", but with l_m / β	"	"	"

1153



1154 Table 5. Average Taylor skill score for the ML+RSL (first number) and CLM4.5 (second
1155 number) simulations. Skill scores greater than those of CLM4.5 are highlighted in bold.

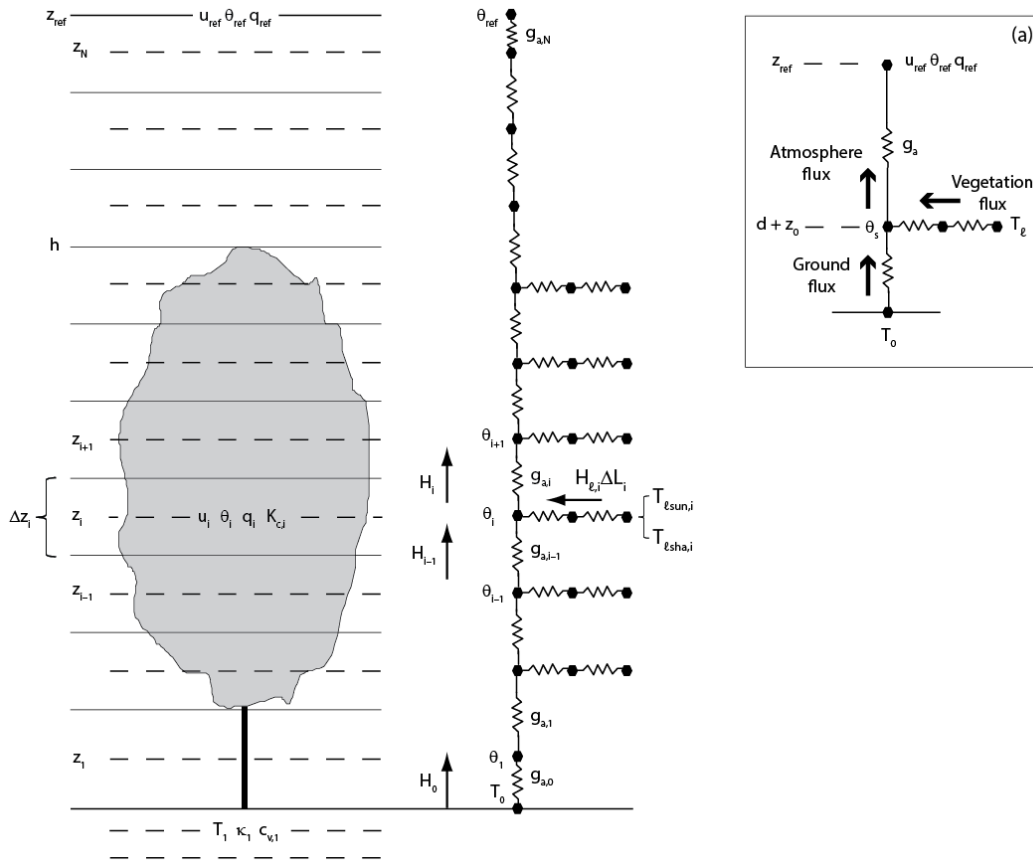
Site	R_n	H	λE	u^*	T_{rad}	GPP
Forest						
US-Ha1	0.98 /0.98	0.89 /0.85	0.94 /0.92	0.91 /0.82	–	0.83 /0.80
US-MMS	1.00 /0.99	0.44/0.47	0.88 /0.87	0.84 /0.78	0.89 /0.81	0.70/0.70
US-UMB	0.99/0.99	0.90 /0.84	0.92 /0.88	0.93 /0.89	0.92 /0.75	0.81 /0.73
US-Dk2	0.98 /0.98	0.53 /0.52	0.93/0.93	0.86 /0.82	0.75 /0.75	–
US-Dk3	0.99 /0.99	0.85 /0.85	0.94/0.94	0.81/0.82	0.83 /0.79	–
US-Ho1	0.96/0.97	0.93/0.94	0.91/0.93	0.92 /0.86	–	0.86/0.87
US-Me2	1.00 /1.00	0.90 /0.79	0.89 /0.64	0.88 /0.84	0.94 /0.78	0.91 /0.57
Herbaceous						
US-Dk1	0.99/0.99	0.89 /0.87	0.90/0.90	0.73/0.82	0.98 /0.95	–
US-Var	0.95/0.96	0.72 /0.59	0.95 /0.95	0.81 /0.79	0.98/0.98	0.89 /0.79
US-Bo1	0.99/0.99	0.75 /0.61	0.96 /0.94	0.94 /0.94	0.90 /0.85	–
US-Ne3	1.00 /1.00	0.48 /0.35	0.85 /0.77	0.98 /0.96	0.94 /0.86	0.78 /0.59
US-ARM	0.96/0.97	0.93 /0.88	0.91/0.94	0.95/0.95	0.98 /0.97	–

1156

1157

1158

1159



1160

1161

1162 Figure 1. Numerical grid used to represent a multi-layer canopy. The volume of air from the
 1163 reference height (z_{ref}) to the ground consists of N layers with a thickness Δz_i , plant area index
 1164 ΔL_i , and plant area density $a_i = \Delta L_i / \Delta z_i$. The canopy has a height h . Wind speed (u_i),
 1165 temperature (θ_i), water vapor concentration (q_i), and scalar diffusivity ($K_{c,i}$) are physically
 1166 centered in each layer at height z_i . An aerodynamic conductance ($g_{a,i}$) regulates the turbulent
 1167 flux between layer i to $i+1$. The right-hand side of the figure depicts the sensible heat fluxes
 1168 below and above layer i (H_{i-1} and H_i) and the total vegetation source flux ($H_{\ell,i}\Delta L_i$) with sunlit



1169 and shaded components. Shown is the conductance network, in which nodal points represent
1170 scalar values in the air and at the leaf. Canopy source fluxes depend on leaf conductances and
1171 leaf temperature, calculated separately for sunlit and shaded leaves using the temperatures $T_{\ell_{sun,i}}$
1172 and $T_{\ell_{sha,i}}$, respectively. The ground is an additional source of heat and water vapor with
1173 temperature T_0 . The inset panel (a) shows the dual-source canopy model used in the Community
1174 Land Model (CLM4.5). Here, Monin–Obukhov similarity theory provides the flux from the
1175 surface with height $d + z_0$ (displacement height plus roughness length) and temperature θ_s to the
1176 reference height with the conductance g_a .

1177

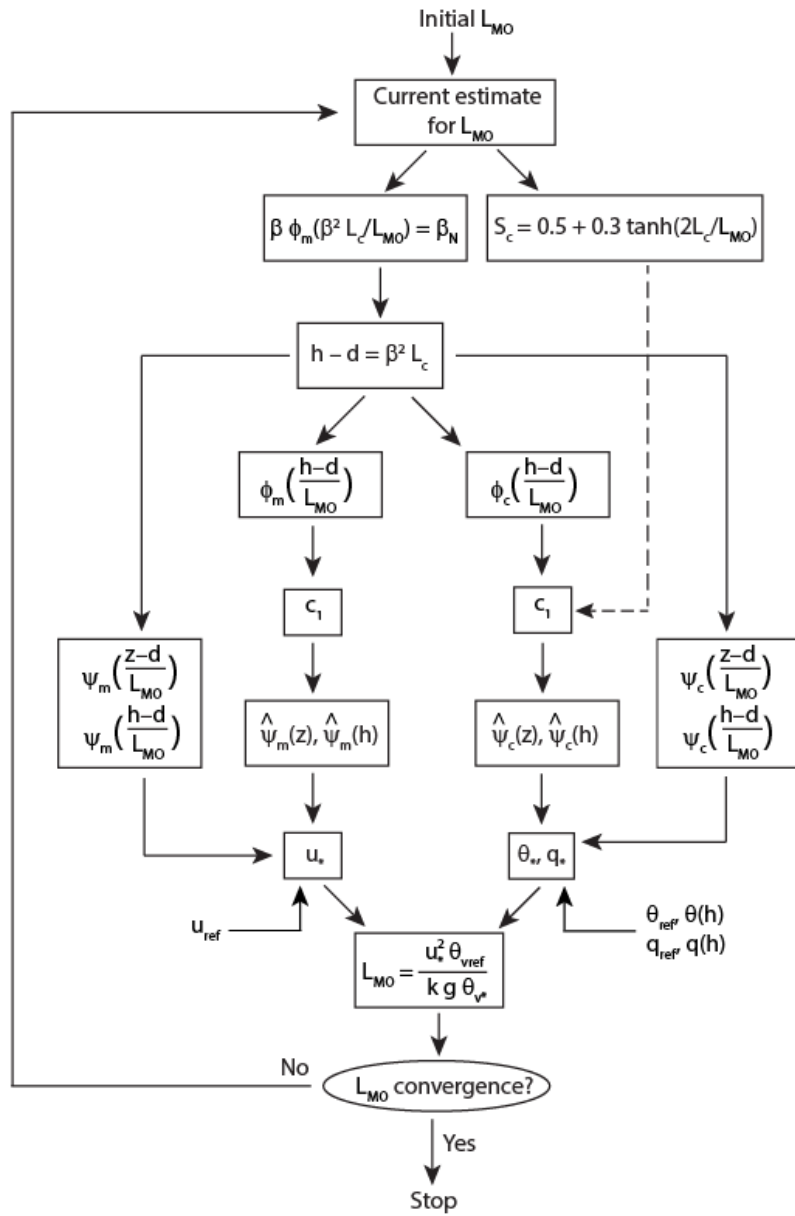
1178

1179

1180

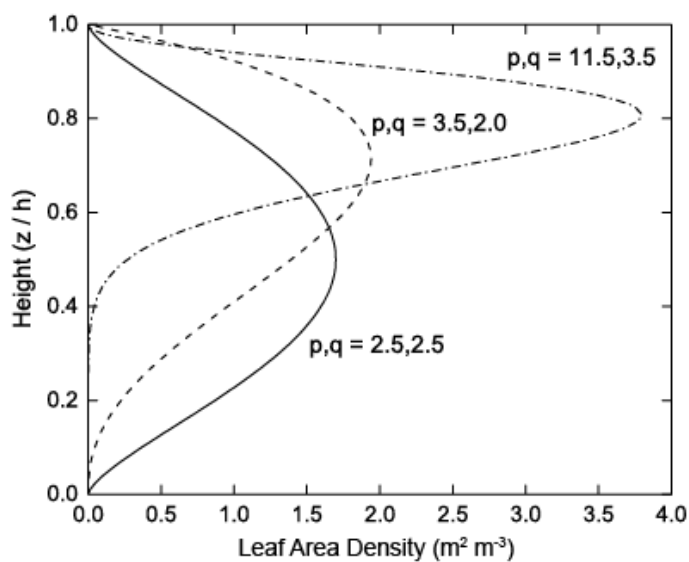
1181

1182



1183
 1184
 1185
 1186
 1187

Figure 2. Flow diagram for calculating the Obukhov length (L_{MO}).



1188

1189 Figure 3. Profiles of leaf area density. Shown are three different canopy profiles for: (i) grass

1190 and crop with $p = q = 2.5$; (ii) deciduous and spruce trees with $p = 3.5$ and $q = 2.0$; and (iii)

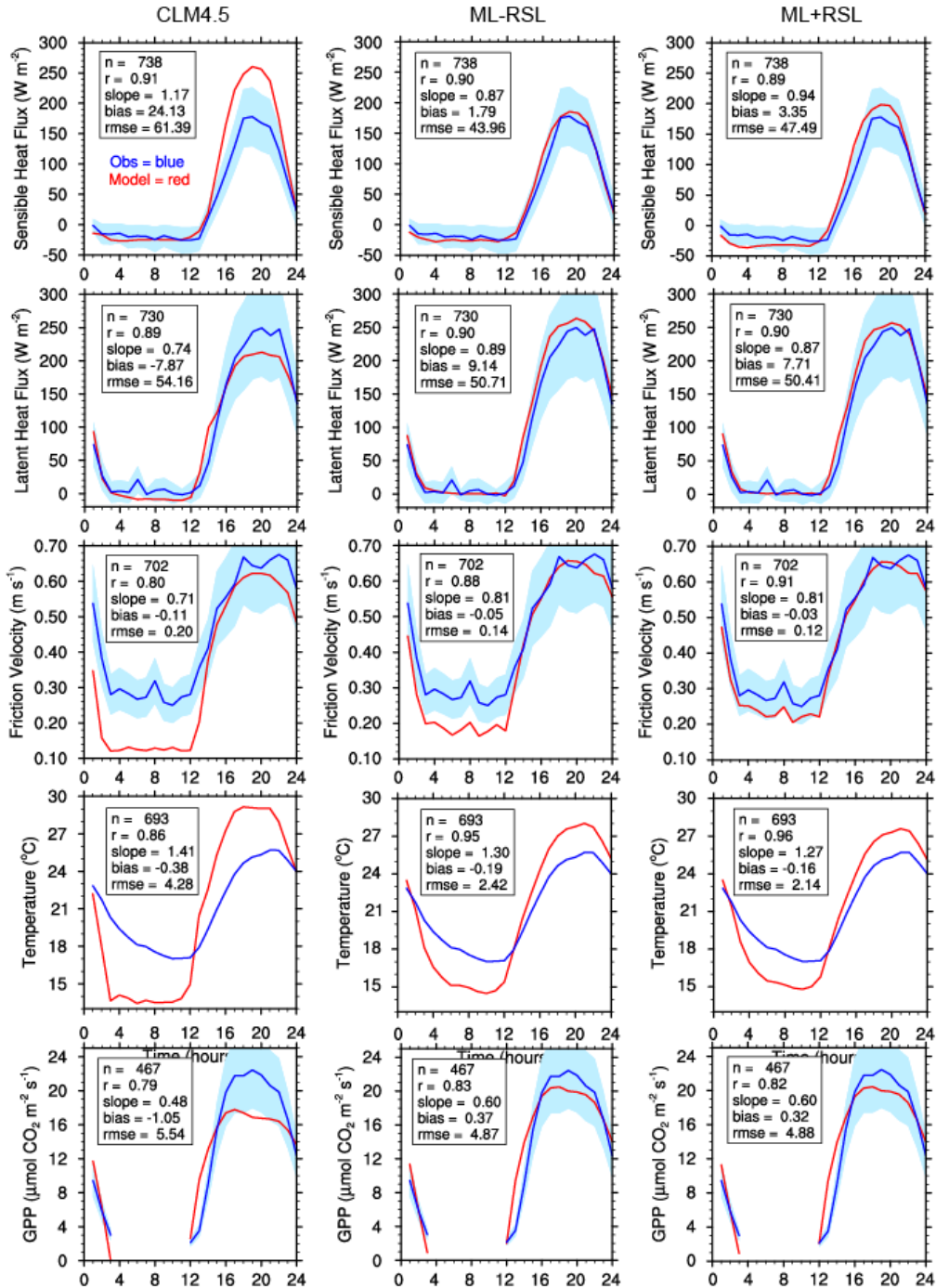
1191 pine trees with $p = 11.5$ and $q = 3.5$. These profiles are show here with $L_r / h = 0.5 \text{ m}^2 \text{ m}^{-3}$.

1192

1193

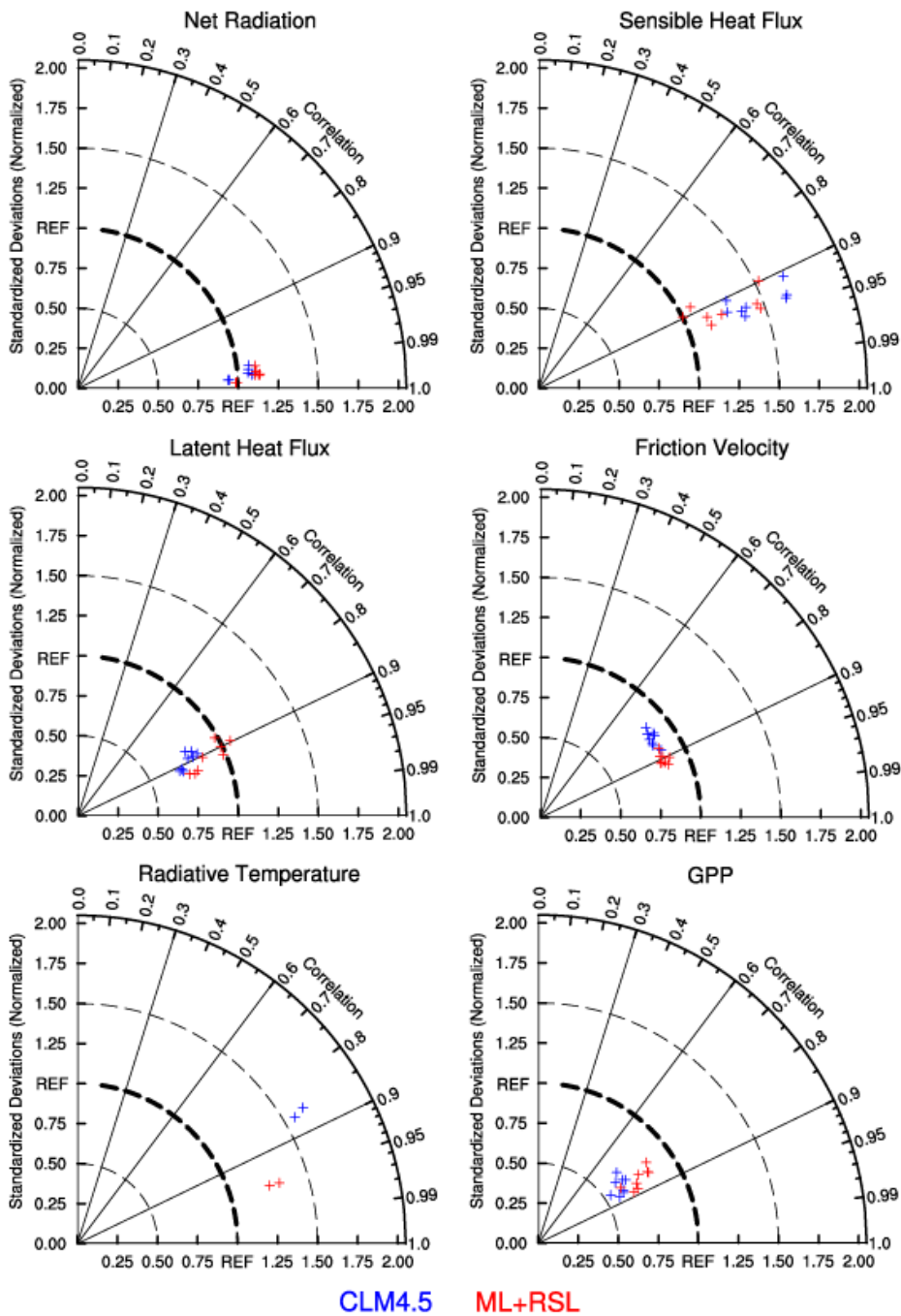
1194

1195





1197 Figure 4. Simulations for US-UMB (July 2006). Shown are the average diurnal cycle (GMT) of
1198 sensible heat flux, latent heat flux, friction velocity, radiative temperature, and gross primary
1199 production (GPP) for the observations (blue) and models (red). The shading denotes ± 1
1200 standard deviation of the random flux error (Richardson et al., 2006, 2012) for H and λE and \pm
1201 20% of the mean for GPP and u_* . Statistics show sample size (n), correlation coefficient (r),
1202 slope of the regression line, mean bias, and root mean square error (rmse) between the model and
1203 observations. Left column: CLM4.5. Middle column: ML-RSL. Right column: ML+RSL.
1204
1205



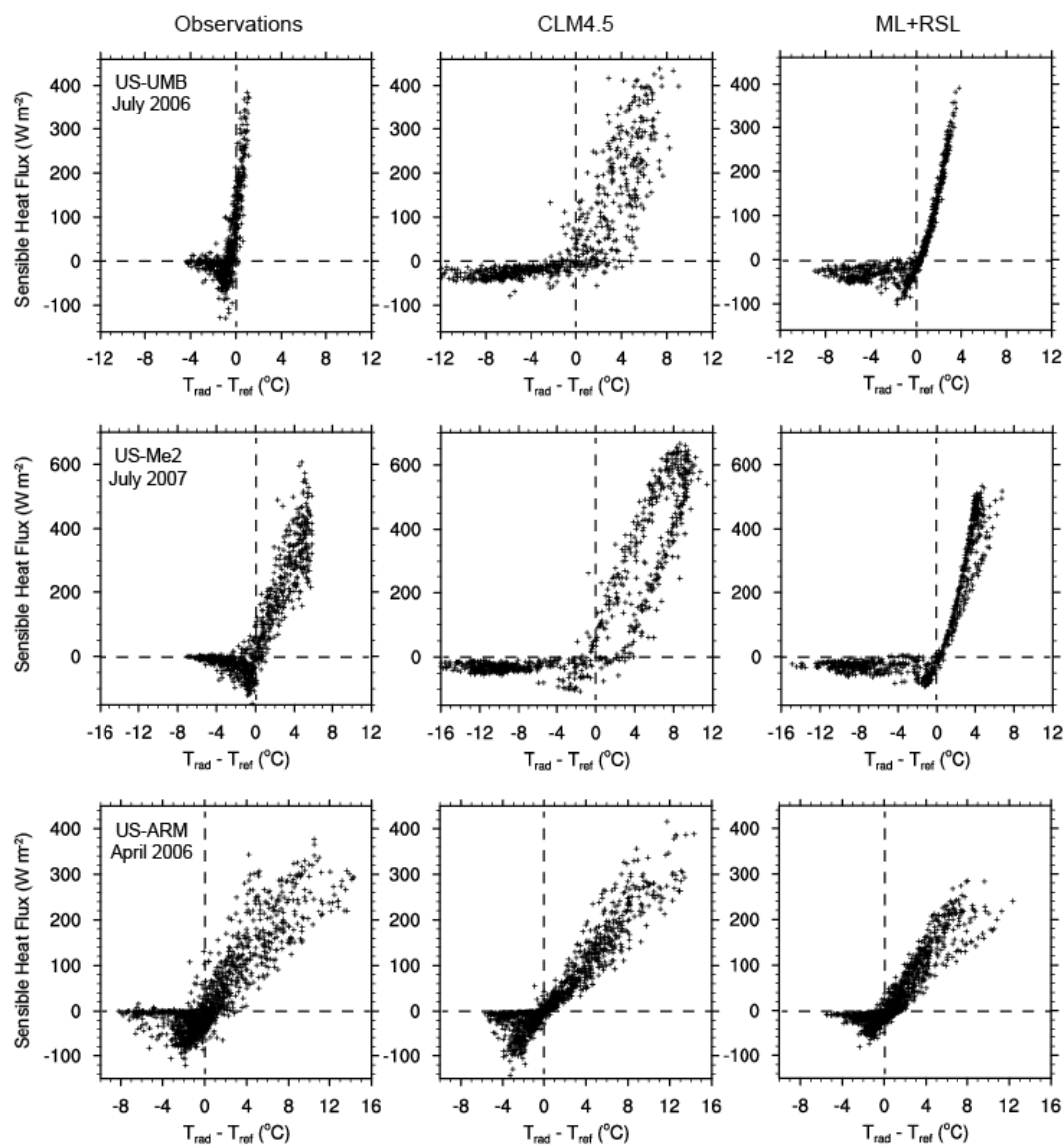
1206



1207 Figure 5. Taylor diagram of net radiation, sensible heat flux, latent heat flux, friction velocity,
1208 radiative temperature, and gross primary production (GPP) for US-UMB. Data points are for the
1209 years 1999–2006 for CLM4.5 (blue) and ML+RSL (red). Simulations are evaluated by the
1210 normalized standard deviation relative to the observations (given by the radial distance of a data
1211 point from the origin) and the correlation with the observations (given by the azimuthal
1212 position). The thick dashed reference line (REF) indicates a normalized standard deviation equal
1213 to one. Model improvement is seen by radial closeness to the REF line and azimuth closeness to
1214 the horizontal axis (correlation coefficient equal to one).

1215

1216



1217

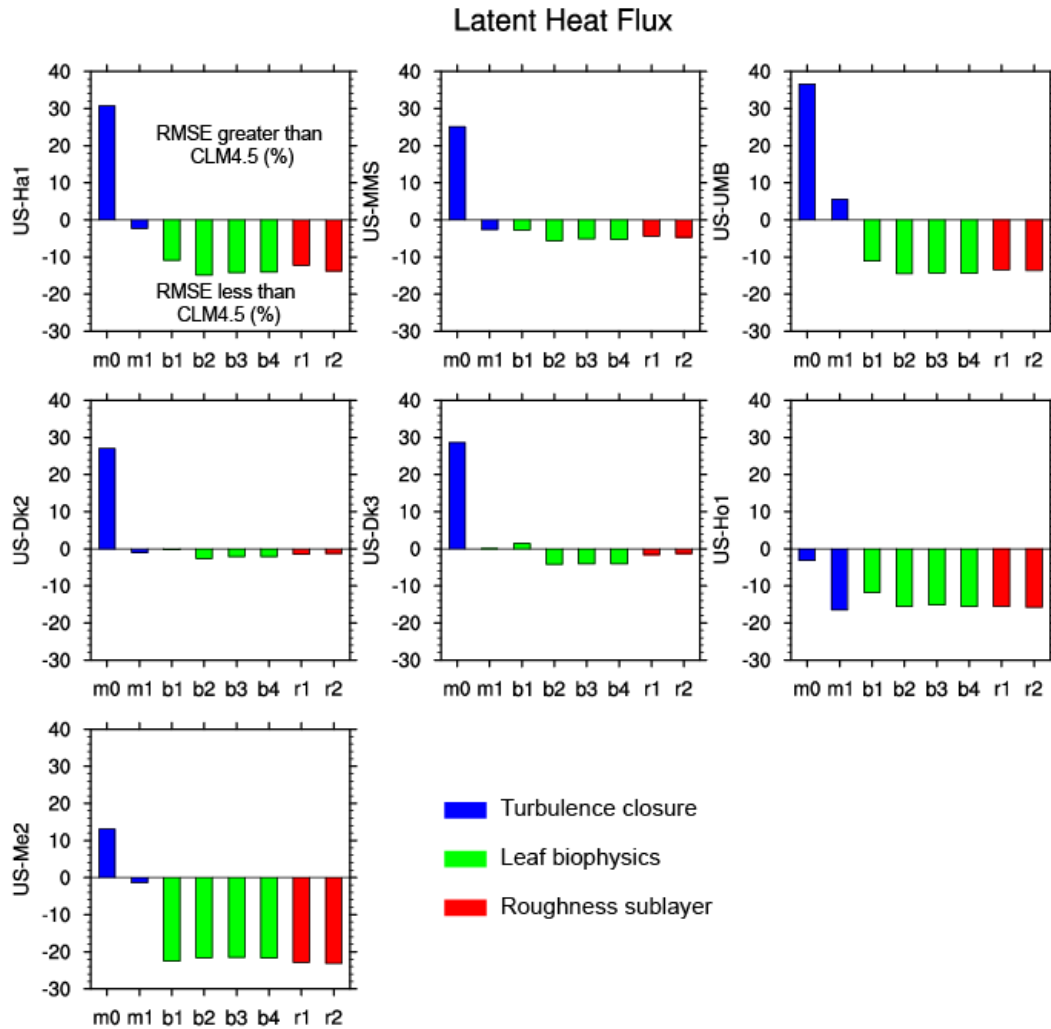
1218 Figure 6. Sensible heat flux in relation to the temperature difference $T_{rad} - T_{ref}$ for US-UMB

1219 (July 2006), US-Me2 (July 2007), and US-ARM (April 2006). Left column: Observations.

1220 Middle column: CLM4.5. Right column: ML+RSL.

1221

1222



1223

1224 Figure 7. Root mean square error (RMSE) for latent heat flux for the 8 simulations m0–r2.

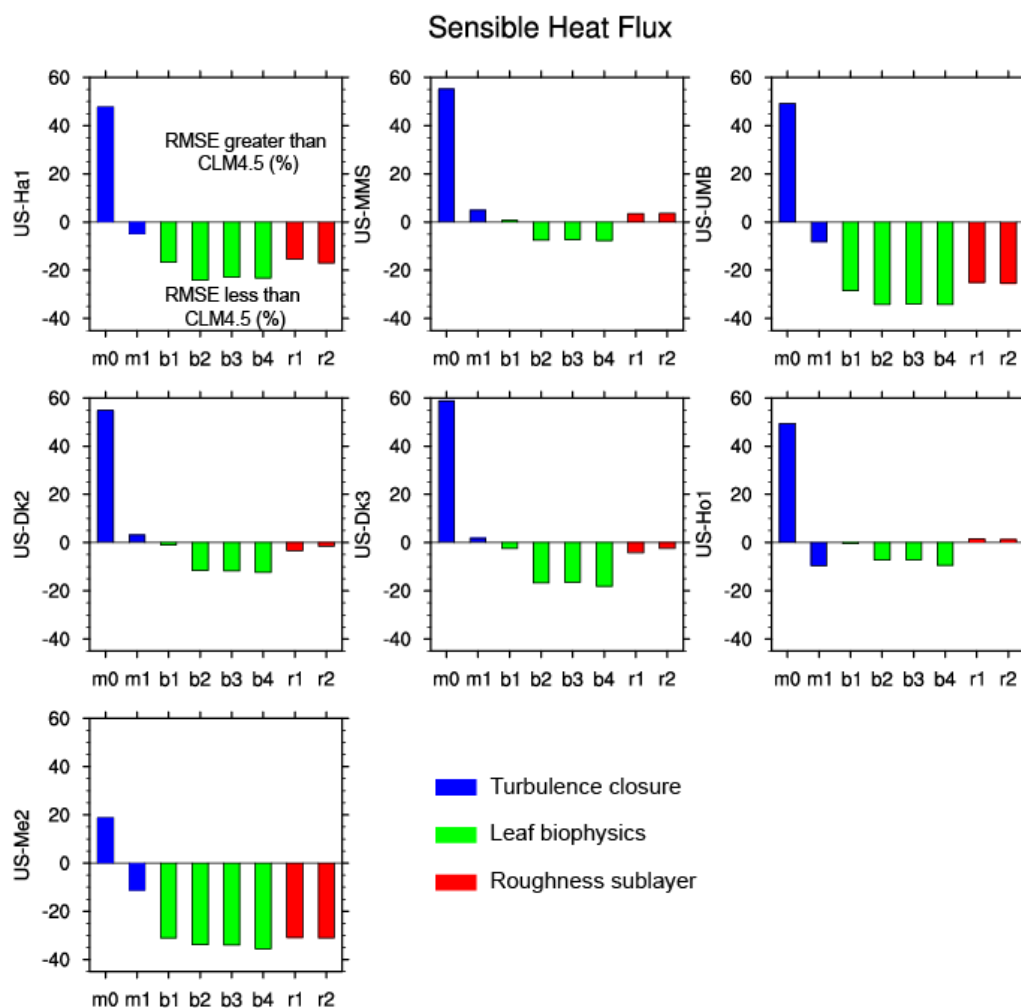
1225 RMSE for each simulation is given as a percentage of the RMSE for CLM4.5 and averaged

1226 across all years at each of the 7 forest sites. Changes in RMSE between simulations show the

1227 effect of sequentially including new model parameterizations as described in Table 4.

1228

1229

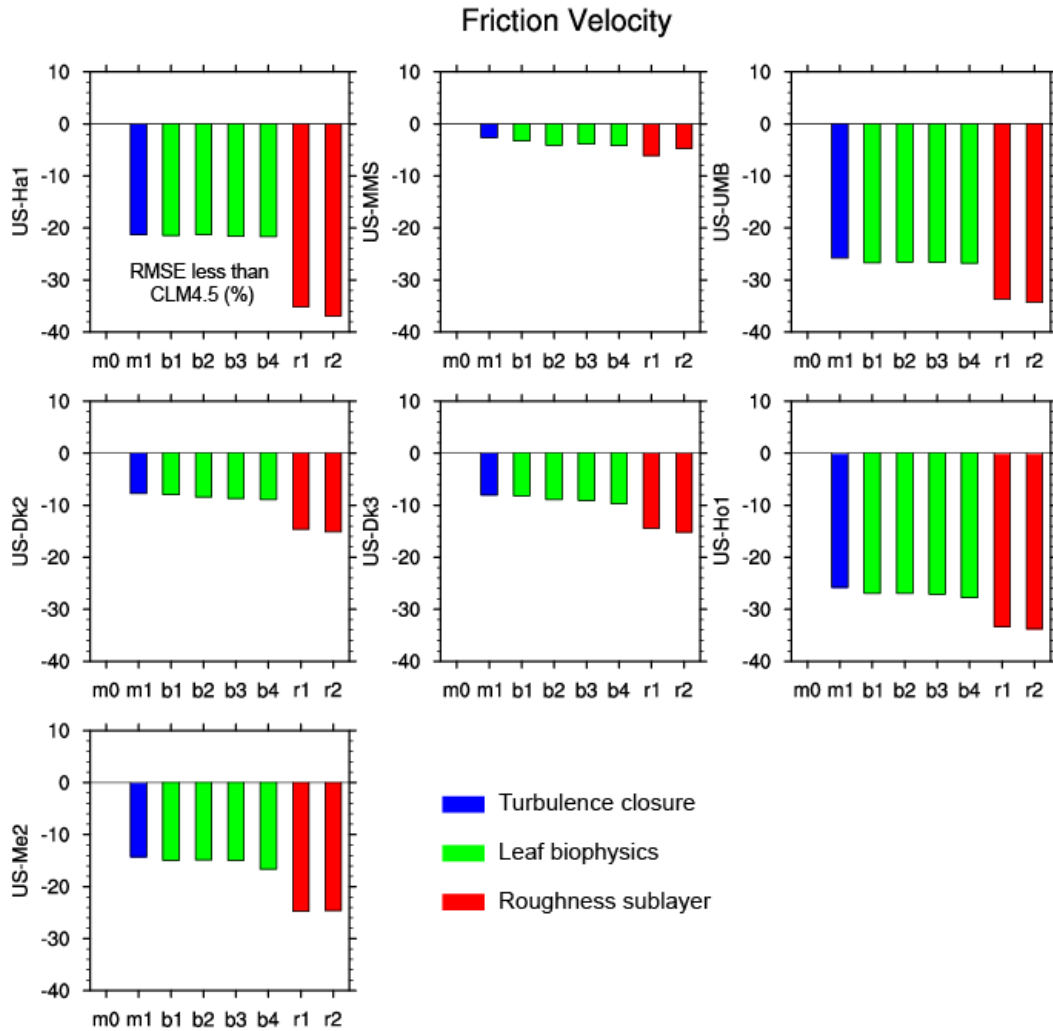


1230

1231 Figure 8. As in Figure 7, but for sensible heat flux.

1232

1233

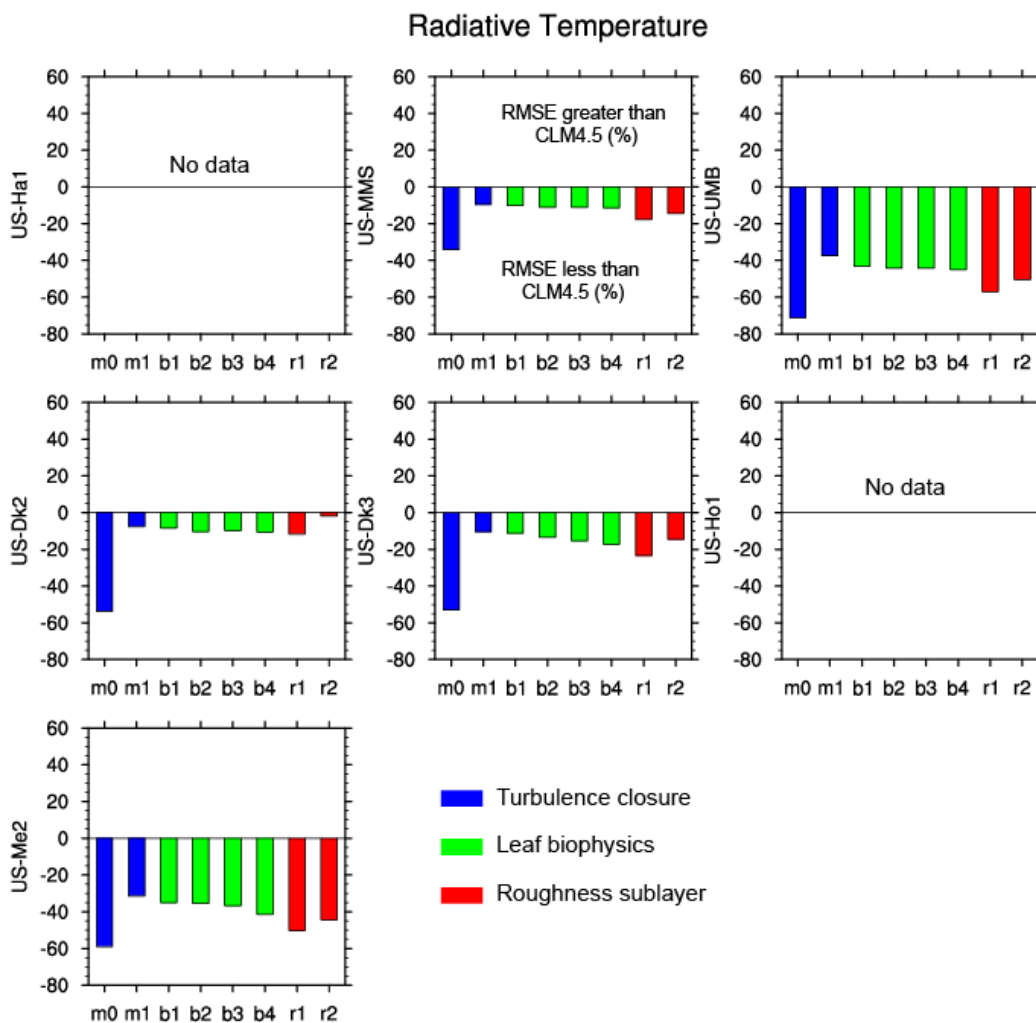


1234

1235 Figure 9. As in Figure 7, but for friction velocity.

1236

1237

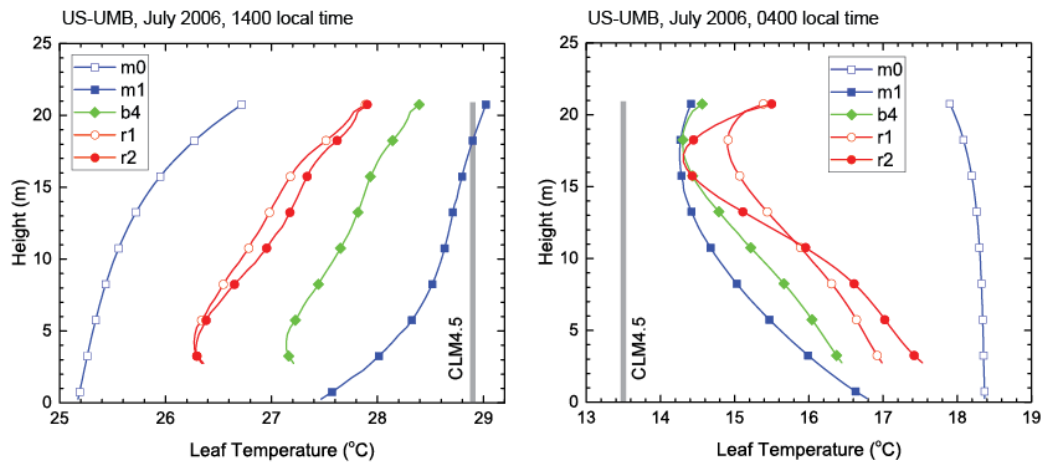


1238

1239 Figure 10. As in Figure 7, but for radiative temperature.

1240

1241

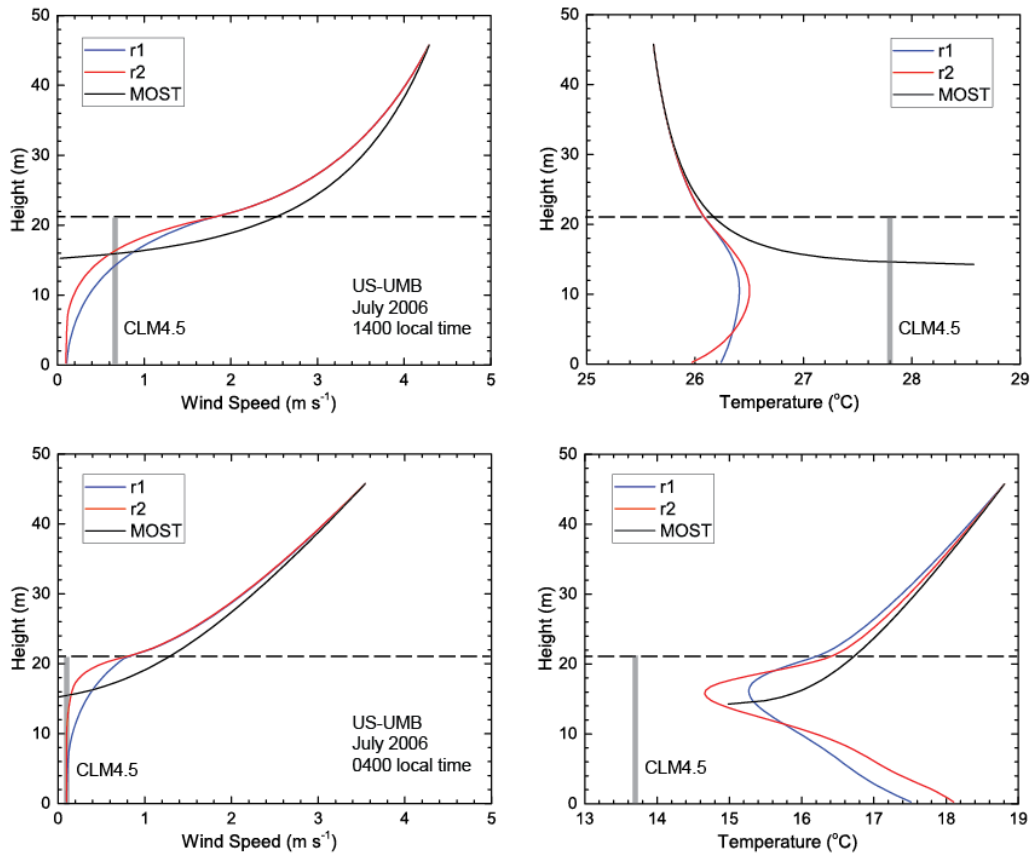


1242

1243 Figure 11. Profiles of leaf temperature for US-UMB averaged for the month of July 2006 at 1400
1244 local time (left panel) and 0400 local time (right panel). Temperature is averaged for sunlit and
1245 shaded leaves at each level in the canopy. Shown are the m0, m1, b4 (ML-RSL), r1, and r2
1246 (ML+RSL) simulations. The CLM4.5 canopy temperature is shown as a thick gray line, but is
1247 not vertically resolved.

1248

1249



1250

1251 Figure 12. Profiles of wind speed and air temperature for US-UMB (July 2006) at 1400 local
1252 time (top panels) and 0400 local time (bottom panels). Shown are the r1 and r2 simulations
1253 averaged for the month. The dashed line denotes the canopy height. The CLM4.5 canopy wind
1254 speed and air temperature are shown as a thick gray line, but are not vertically resolved. Also
1255 shown are the profiles obtained using MOST extrapolated to the surface. This extrapolation is for
1256 the r2 simulation using Eqs. (19) and (20) but without the RSL and with roughness length and
1257 displacement height specified as in the CLM4.5.

1258